Development of an Analytical Automotive Damper Model

Undergraduate Honors Thesis

Presented in Partial Fulfillment of the Requirements for

Graduation with Distinction

at The Ohio State University

By

Ben Thornton

* * * * *

The Ohio State University

2011

Defense Committee:

Professor Marcelo Dapino
Advisor

Professor Yann Guezennec

Approved by

Adviser

Undergraduate Program in
Mechanical Engineering

ABSTRACT

Physical models are tools that are commonly used in the automotive industry. Accurate models exist for most automotive systems. However, few accurate models have been developed to model the individual components of the damper. This document describes the development of a physical model based on the parameters of two automotive dampers provided by Honda R&D. The model is derived from four considerations. These are Newton's second law, fluid continuity, fluid compressibility, and orifice flow. The main challenge of developing this model was to accurately evaluate the parameters of the dampers. Two parameters that are focused on in this document are check valve stiffness and bulk modulus. These parameters were determined experimentally. The methods used to determine these parameters are described in detail in this document.

ACKNOWLEDGEMENTS

I would like to express my sincere gratitude to Professor Marcelo Dapino for providing with me with the resources and guidance that allowed me to complete this thesis. Your expertise in the field was greatly appreciated throughout the course of this project.

I would like to thank Tony King for working side by side with me on this project. Tony made significant contributions to the project which helped keep the project on schedule while maintaining high standards of quality. Thank you to Brian Schoeny and Showa R&D for the time and resources that were devoted to this project.

Finally, I would like to thank John Yu, Kirk Rhoads, and Bryan Johnson from Honda R&D for providing your time and expertise. I am honored to be able to carry out a project for such a prestigious research facility.

TABLE OF CONTENTS

TABLE OF FIGURES

CHAPTER 1: INTRODUCTION

1.1 Motivation

The automotive industry has become one of the most competitive industries of today's economy. Over 77 million automobiles were produced in 2010 alone (International Organization of Motor Vehicle Manufactures, 2011). Efficient use of time and resources is crucial in such an industry. A tool that has significantly improved the efficiency of the automotive design process is physical modeling of the automobile. Theoretical physical models help engineers to better understand exactly how automotive systems work. Insight to how these systems work ultimately leads to the ability to improve upon them. Automotive companies have invested massive amounts of resources into research that aims to model the dynamics of an automobile using physical mathematical equations. To do this the automobile is broken down into numerous systems. Each of these systems can be characterized using several equations. Many of these systems can be characterized quite accurately using physically intuitive equations. The damper, however, seems to be an exception.

There is an overt need in the automotive industry for an accurate physical damper model that can be used in larger vehicle system models and as an individual tool for damper design. Unfortunately, few physical damper models exist in scholarly literature. A major reason for this is that the damper is characterized by phenomena that are difficult to predict theoretically without empirical knowledge of certain variables such as friction coefficients, discharge coefficients, and effective stiffness values of various parts. In the absence of a true physical damper model engineers have developed other methods of damper design. Many of these methods involve trial and error. Trial and error methods have been replaced in most other areas

of automotive design due their inherent inefficient use of time as well as their lack of precision. It is possible that this method prevails in damper design because it is highly compatible with the subjective methods used to evaluate passenger comfort. In spite of this advantage of the trial and error method, a better understanding of the physical processes that take place in the damper would be extremely beneficial to the damper design process.

1.2 Project Objectives

The objective of this study is to create a physical analytical damper model that can be validated experimentally with 80% accuracy. This model will calculate the force output from the damper based on a dynamic input displacement. The model will be based on parameters of a specific damper model. However, the governing equations must be applicable to two different Honda damper models while maintaining 80% accuracy during validation. The parameters of the model are obtained using various theoretical and empirical methods which are described in this report.

1.3 Background

An important part of the automotive suspension is the damper. This is the device that dissipates unwanted vertical and lateral energy from the automobile. If the suspension consisted only of a spring with no energy dissipation, any input to the system would result in perpetual harmonic motion. Energy would convert between kinetic energy and potential energy but would never leave the system. The damper converts kinetic energy to thermal energy thus effectively dissipating it from the system.

The dampers used in this study are dual tube dampers. As can be seen in Figure 1, these dampers consist of three chambers. These are the rebound, compression, and reserve chambers.

For the purpose of this paper these three chambers will be denoted as chamber 1, chamber 2, and chamber 3 respectively. Chambers 1 and 2 consist entirely of hydraulic oil and are separated by a piston attached to the damper rod. Most of the viscous damping is generated by flow of oil between chambers 1 and 2 through orifices in this piston. Chamber 3 makes up the space between the inner and outer tubes. This chamber consists of nitrogen gas and hydraulic oil which are separated by gravity. The purpose of chamber 3 is to allow the rod to be inserted into chamber 1 without creating a large increase in pressure. When the rod is inserted, the nitrogen in chamber 3 compresses to account for the change in volume caused by the insertion of the rod. Due to the low bulk modulus of nitrogen gas, the rod can be inserted without significantly increasing the internal pressure of the damper.

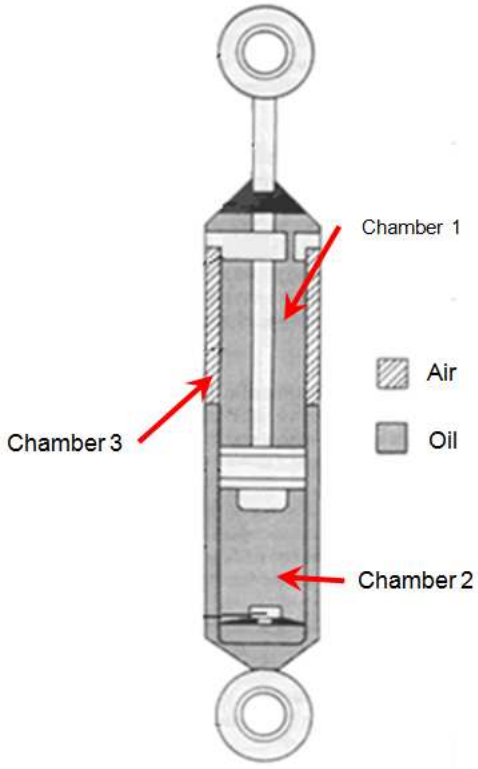

Figure 1: Diagram of Dual Tube Damper (Lang, 1977)

The characteristics of the piston orifices play a large role in the dynamics of the damper. They control the flow of hydraulic oil from chamber 1 to 2. There are two types of orifices in the damper piston. One of these orifices is a constant area bleed valve. This orifice is open regardless of pressure and allows flow in both directions. The piston also contains two variable area check valves. This valve is different from the bleed valve in several ways. Unlike the bleed valve, the check valve closes at low pressure differentials. Also, each check valve will only allow flow in one direction. Lastly, the cross sectional area of the check valve changes depending upon the pressure difference across the valve.

These check valves are made up of orifices sealed at one opening by circular cantilevered shims. These can be seen in Figure 2. As the difference in pressure across the valve increases, more force is applied to the shim. This force causes the shim to deflect allowing flow through the orifice. The orifice area is directly related to the deflection of the shim and therefore the pressure differential.

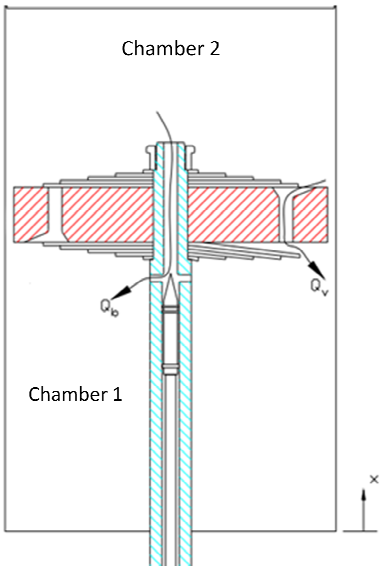

Figure 2: Diagram of Damper Piston Valves (Talbott, et al., 2002)

CHAPTER 2: LITERATURE REVIEW

There were several goals in mind during the conduction of the literature review. One goal was to identify the damper parameters that are relevant for creating an accurate parametric model. The second goal of the literature review was to investigate the various methods that have been used in the past for measuring these parameters. Each of the relevant parameters that were identified in the literature research is discussed in this section.

2.1 Valve Characterization

Many researchers including Lang (Lang, 1977) and Talbott (Talbott, et al., 2002) have modeled the characteristics of damper valves using equations for orifice flow. The areas of these orifices were modeled as functions of shim displacement. Talbott also developed analytical equations for shim stiffness using formulas from Roark.(Warren, et al., 1989) One drawback of this method was that the location at which the fluid pressure is effectively acting on the shim is unknown. Talbott chose a value that best fit his experimental data.

In 2007 Shams (Shams, et al., 2007) published an article researching a much more sophisticated method of characterizing damper valves. Shams used FEA and CFD to model the characteristics of damper valves. Shams created a 3D CFD model of the valve. Shams conducted simulations for seven different shim deflections. For each shim deflection the simulation was conducted for six different piston velocities. This simulation provided a relationship between resultant shim force and shim deflection for various piston velocities. Shams then conducted an FEA simulation to determine the relationship between resultant force on the shim and displacement of the shim. These two relationships were coupled to determine the relationship between piston velocity and shim deflection.

2.2 Fluid Compressibility

In 2004 Lee and Sun (Lee, et al., 2004) developed equations for the effective bulk modulus of the fluid in a damper. This effective bulk modulus accounts for the compliance of all the internal components of the damper. This includes the fluid, gas, and chamber. Lee and Sun determined the bulk modulus of the fluid experimentally. The gas was modeled using the ideal gas equations. Lee and Sun's most significant contribution was their analytical methods of determining the effective bulk modulus of the chambers of the damper. Using these methods they showed that the compliance of the damper chamber is significant in comparison to the bulk modulus of the fluid.

There are many methods that have been used in the past for measuring the bulk modulus of a fluid. Many of these methods involve measuring the speed of sound through the fluid. The speed of sound is directly related to the bulk modulus and the density. If the density and the speed of sound are both known the bulk modulus can be determined. Balasubramanian (Balasubramanian, 2003) presents a method of measuring the speed of sound through a fluid. Balasubramanian used a plunger to apply pressure pulses to the fluid in a rigid container. Three pressure transducers were installed at various distances from the plunger. The time lag between the signals measured by each of these pressure transducers could be used to determine the speed of sound through the fluid.

2.3 Dynamic Discharge Coefficient

In Lang's thesis (Lang, 1977) he experimentally determined dynamic discharge values for all the valves in a specifi. He correlated these dynamic discharge values with acceleration number as well as Reynold's Number. The results of his research showed that the dynamic discharge coefficients for each of the valves were very close to 0.7. Many subsequent studies

including Rhoads (Rhoades, 2006) and Talbott (Talbott, et al., 2002) have used 0.7 as a starting point and later adjusted the dynamic discharge coefficient such that a better correlation could be achieved between the model and the data.

CHAPTER 3: ANALYTICAL MODEL

Figure 3 shows the diagram that was used to derive the analytical damper equations. The governing equations for this model are based on four considerations. These are Newtons's second law, fluid continuity, orifice flow, and fluid compressibility.

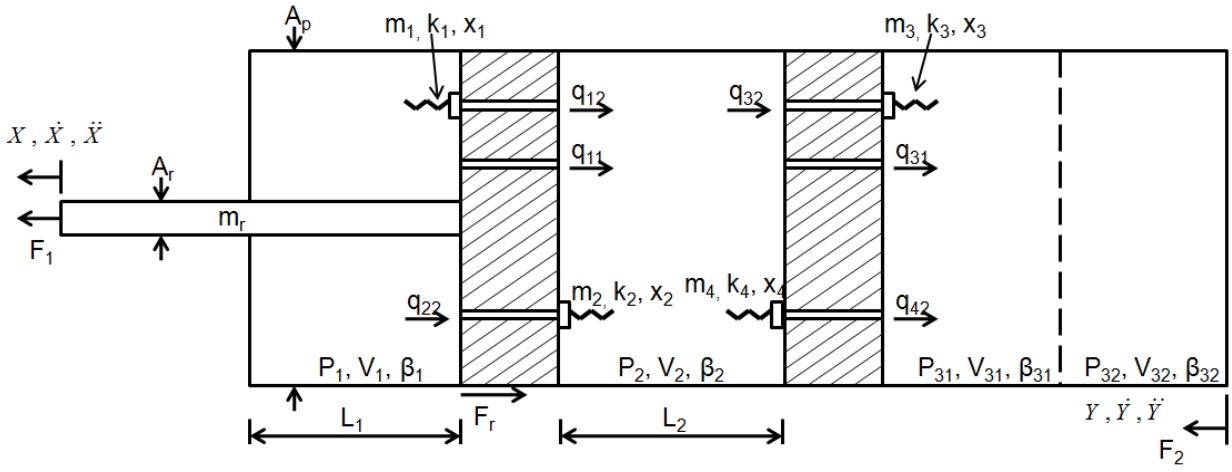

Figure 3: Diagram of Analytical Damper Model

Force Balance Equations:

Unlike other damper models, this model takes into consideration the movement of the damper as well as the movement of the piston instead of considering only the movement of the piston. This is more beneficial than assuming that the damper body is fixed and the piston is moving for two reasons. One is that during experimental testing the piston and rod are fixed while motion is excited in the damper body. Another reason is that during actual use the damper body and the piston are both moving independently. This effect could not be modeled without considering the motion of both components.

In order to account for both piston and body movement a separate force balance equation was developed for the piston and for the body. The difference between the external forces acting upon the damper body and piston rod will be due solely to the difference in inertia between the damper body and the piston. These two force balances are shown in Equations 1-2.

$$F_1 = m_r\ddot{X} - p_2A_p + p_1\left(A_p - A_r\right) + F_r sgn(\dot{z}) \tag{1}$$

$$F_2 = m_b\ddot{X} + p_2A_p - p_1\left(A_p - A_r\right) - F_r sgn(\dot{z}) \tag{2}$$

Chamber 1 Continuity Equation:

This equation simply states that the sum of flows in or out of the chamber in addition to the change in volume due to fluid compressibility is equal to the total change in volume of the chamber. Each of the flow variables is defined in the following sections.

$$q_{11} + q_{12} + q_{22} + q_{\beta 1} = \dot{z}\left(A_p - A_r\right) \tag{3}$$

Chamber 1 Orifice Flow Equations:

The bleed valve was modeled using a constant area orifice flow equation.

$$q_{11} = n_{11}C_{d11}A_{11}sgn(p_1 - p_2)\sqrt{\frac{2|p_1 - p_2|}{\rho}} \tag{4}$$

The design of the check valves allows flow in only one direction. A piecewise function was used to model this. The piecewise function sets the flow to zero instead of allowing flow in the reverse direction.

$$q_{12} = \begin{cases} 0, & p_1 \geq p_2 \\ -C_{d12}A_{12}\sqrt{\frac{2|p_1 - p_2|}{\rho}}, & p_1 < p_2 \end{cases} \tag{5}$$

$$q_{22} = \begin{cases} 0, & p_1 \leq p_2 \\ C_{d22} A_{22} \sqrt{\dfrac{2|p_1 - p_2|}{\rho}}, & p_1 > p_2 \end{cases} \tag{6}$$

Chamber 1 Fluid Compressibility Equations:

The change in volume of the fluid due to fluid compressibility is derived from the equation for fluid bulk modulus. The bulk modulus is a function of pressure that will be determined experimentally.

$$q_{\beta 1} = \frac{(L_1 - z)\left(A_p - A_r\right)}{\beta_1} \dot{p}_1 \tag{7}$$

$$\beta_1 = \beta_1(p_1) \tag{8}$$

Chamber 1 Orifice Area Equations:

$$A_{12} = \pi D_{v12} x_1 \tag{9}$$

$$A_{22} = \pi D_{v22} x_2 \tag{10}$$

The displacement of the shim is related to the force and the stiffness. The force is equal to the product of the pressure differential and the effective area on which this pressure differential acts. This area is assumed to be the product of the orifice area and the number of orifices.

$$x_1 = \frac{|p_1 - p_2| * A_{f12} n_{12}}{k_1} \tag{11}$$

$$x_2 = \frac{|p_1 - p_2| * A_{f22} n_{22}}{k_2} \tag{12}$$

Chamber 2 Continuity Equation:

$$q_{11} + q_{12} + q_{22} - q_{\beta 2} - q_{31} - q_{32} - q_{42} = \dot{z}A_p \tag{13}$$

Chamber 2 Orifice Flow Equations:

$$q_{31} = n_{31}C_{d31}A_{31}sgn(p_2 - p_3)\sqrt{\frac{2|p_2 - p_3|}{\rho}} \tag{14}$$

$$q_{32} = \begin{cases} 0, & p_3 \geq p_2 \\ C_{d32}A_{32}\sqrt{\frac{2|p_2 - p_3|}{\rho}}, & p_3 < p_2 \end{cases} \tag{15}$$

$$q_{42} = \begin{cases} 0, & p_3 \leq p_2 \\ -C_{d42}A_{42}\sqrt{\frac{2|p_2 - p_3|}{\rho}}, & p_3 > p_2 \end{cases} \tag{16}$$

Chamber 2 Fluid Compressibility Equations:

$$q_{\beta 2} = \frac{(L_2 + z)A_p}{\beta_2}\dot{p}_2 \tag{17}$$

$$\beta_2 = \beta_2(p_2) \tag{18}$$

Chamber 2 Orifice Area Equations:

$$A_{32} = \pi D_{v32}x_3 \tag{19}$$

$$A_{42} = \pi D_{v42}x_4 \tag{20}$$

$$x_3 = \frac{|p_2 - p_3| * A_{f32}n_{12}}{k_3} \tag{21}$$

$$x_2 = \frac{|p_2 - p_3| * A_{f42}n_{42}}{k_4} \tag{22}$$

Chamber 3 Continuity Equations:

$$q_{31} + q_{32} + q_{42} - q_{\beta 31} - q_{\beta 32} = 0 \tag{23}$$

$$V_{31} + V_{32} = V_3 \tag{24}$$

Chamber 3 Fluid Compressibility Equations:

$$q_{\beta 31} = \frac{V_{31}}{\beta_{31}} \dot{p}_3 \tag{25}$$

$$q_{\beta 32} = \frac{V_{32}}{\beta_{32}} \dot{p}_3 \tag{26}$$

Chamber three is unique to the other chambers in that its volume is fixed. However, the individual volumes of gas and oil within chamber three are not fixed. Equation 27 allows the model to relate the volume of gas within chamber 3 to the pressure of chamber 3. Because chamber three has a constant volume there is a known relationship between the volume of gas in chamber three and the volume of oil in chamber three.

$$V_{32} = V_{32_0}(1 - \frac{p_3 - p_{3_0}}{\beta_{32}}) \tag{27}$$

$$\beta_{31} = \beta_{31}(p_3) \tag{28}$$

CHAPTER 4: SHIM STIFFNESS

Three methods of determining shim stiffness were considered. These three methods are analytical, FEA, and experimental. Each of these methods has certain drawbacks. Analytical equations for shim stiffness have been developed and are defined in *Roark's Formulas for Stress and Strain*. (Warren, et al., 1989) Unfortunately, the irregular loading that is seen by the shim cannot be modeled using these equations. Furthermore, these equations are not able to model the effects of friction between the individual shims. The friction effects were also unable to be accurately modeled using FEA. An option that was investigated was to model the shim stack as a solid body. The results of this model, which are presented in this chapter, show that this is not a valid approximation. The most viable option for characterizing the shim stiffness proved to be experimental methods. However, this method also had drawbacks. The main drawback being that the loading on the shim cannot be easily recreated in an experiment. For this reason the experiments conducted for shim stiffness characterization used simplified loading patterns. Despite this inaccuracy, the experimental method was chosen as the main method of characterizing the shim stiffness.

4.1 FEA Validation Test

Finite element analysis is one option that was considered for characterizing the stiffness of the valve shims. One of the challenges encountered using this method was to experimentally validata the results of a finite element analysis. This could only be done for a test that can be setup up and measured in realty and in an FEA simulation. It was not practical to recreate the loading of the shims in this way. Instead, a simplified loading pattern was used. This loading pattern could be applied in an experimental setup and in the FEA setup. If an FEA simulation

could be validated using this loading pattern it could be assumed that the solid model and boundary conditions used were correct. At this point the simplified loading pattern could be replaced by a more accurate representation of the loading to which the shims are subjected in the damper.

The simplified loading pattern used was a ring load. The solid model incorporated several simplifying assumptions. It assumed that the shims were one solid body rather than modeling the boundaries between each shim. This was done because of the difficulty of accurately modeling friction between the shims without empirical friction data. The model was also simplified to a 2D model with axis-symmetric conditions. Figure 4 shows this FEA model.

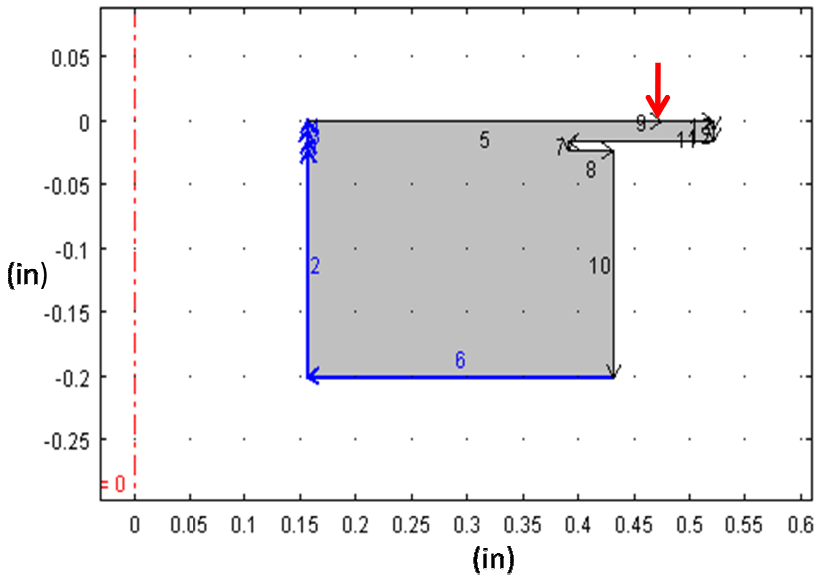

Figure 4: FEA Validation Test: Simulated Setup

A fixture was designed to apply a ring load at precisely the same diameter as in the FEA. This diameter was 0.950 in. The fixtures used in the experimental setup are shown in Figure 5. The shim and fixture stiffness curves obtained experimentally are shown in Figure 6. The

resulting shim stiffness values are shown in Table 1. See section 4.2.1 *Experimental Setup* for a description of the method used to obtain the shim stiffness.

Figure 5: FEA Validation Test: Fixtures for Experimental Setup

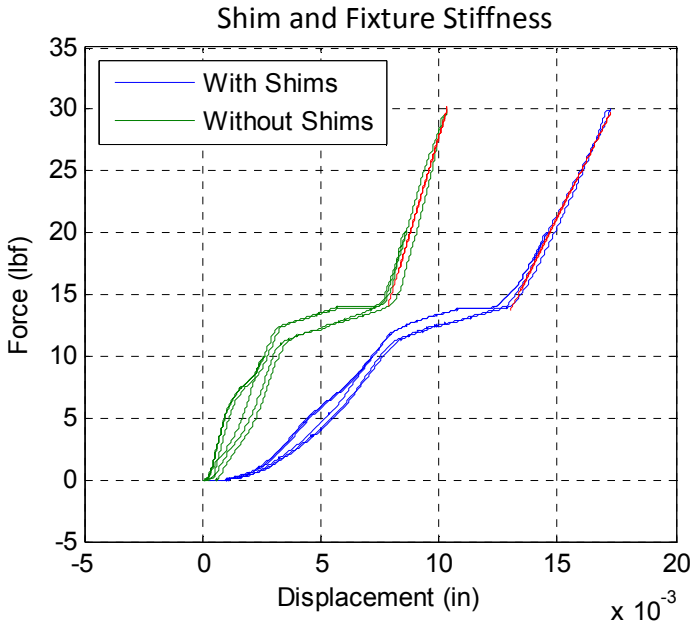

Figure 6: FEA Validation Test: Experimental Results

Table 1: FEA Validation Test Experimental Results

Component	Stiffness (lb/in)
Fixture	6390.5
Fixture and Shims in Series	3773.4
Isolated Shims	9214.0

The experimental stiffness values are compared to the FEA stiffness values in Figure 7 and in Table 2. The FEA simulation was evaluated using COMSOL and SolidWorks. The results of the two simulations matched moderately well. However, the experimental results matched the FEA results poorly. This lead to the conclusion that the assumptions made in the FEA model are not valid. Specifically, the assumption that the shims can be modeled as a single solid body is invalid. Once the results of the FEA validation test proved that the simplifying assumptions were invalid, experimental methods for characterizing the shims were considered.

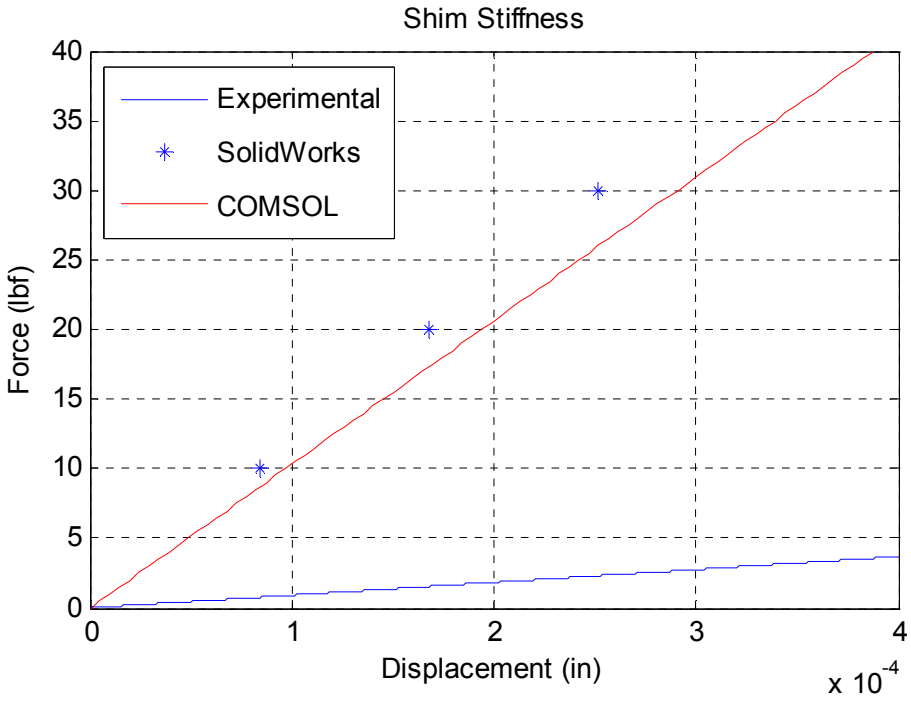

Figure 7: FEA Validation Test: Comparison of FEA and Experimental Results

Table 2: FEA Validation Test: Comparison of FEA and Experimental Results

Method	Stiffness (lb/in)	% Difference (%)
COMSOL	1.032×10^5	--
SolidWorks	1.1915×10^5	15.5
Experimental	9.214×10^3	91.1

4.2 Experimental Shim Characterization

The main difficulty when characterizing the stiffness of the shims experimentally is recreating the loading of the shim in a measurable test. Applying a fluid pressure to the shims would make the shims inaccessible. Access to the shims is required for measuring the displacement of the shims. Another option that was considered was to make forks whose prongs had cross sections similar to the cross sections of the piston orifices. These prongs could be pressed against the surface of the shim to recreate the force of the fluid pressure. The drawback to this option is that parts of the prong would lose contact with the shim as the shim deflects. At any significant deflection only the inner edge of the prong would still be in contact. This effect is shown in Figure 8.

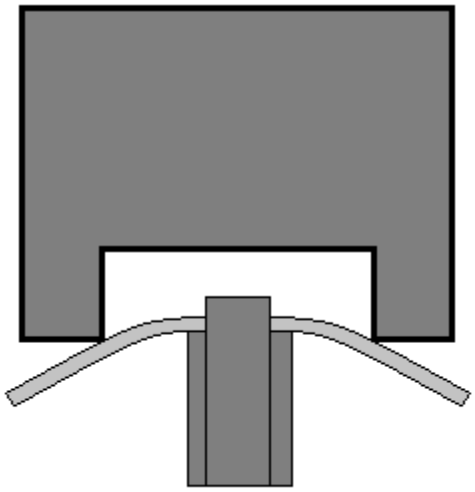

Figure 8: Diagram of Shims Loosing Contact with Fork Prongs

To prevent this effect from taking place the loading pattern had to be simplified. Orifices with circular cross sections were simplified to point loads while orifices with rectangular cross sections were simplified to line loads. Some accuracy would be lost in this simplification. However, this simplification allowed precise control over the location of the applied load. This section describes this experiment.

4.2.1 Experimental Setup

The loading forks that were used in this experiment are shown in Figure 9 and Figure 10. For each valve the valve body is shown to the left and the fork designed to imitate the load is shown on the right. The entire experimental setup is shown in Figure 11.

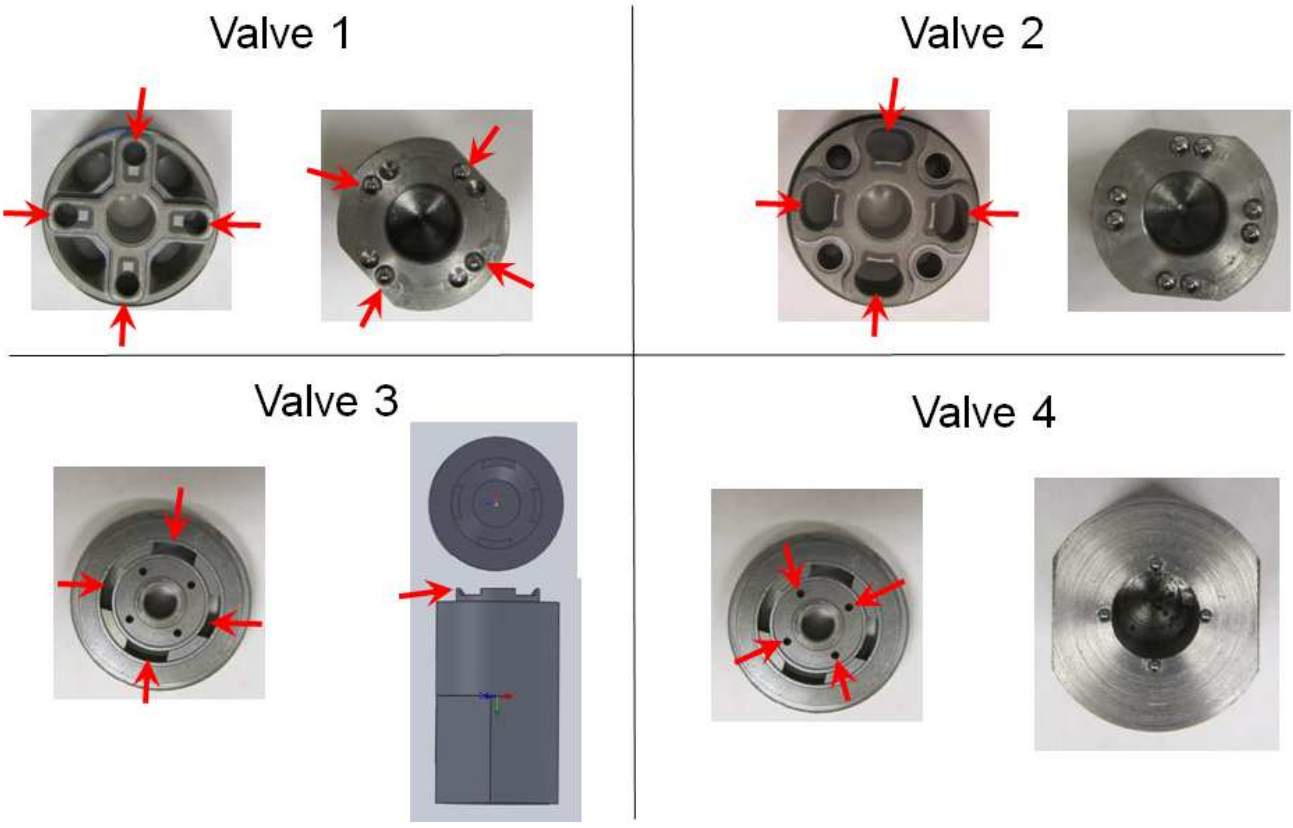

Figure 9: SZA Load Forks

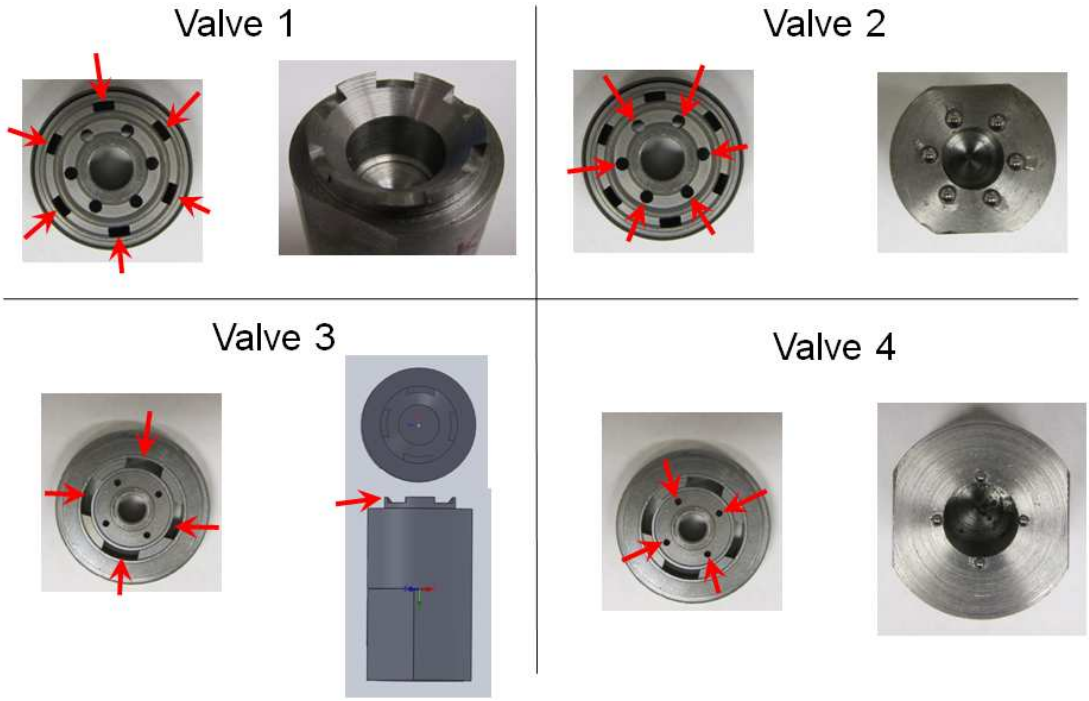

Figure 10: TK8 Load Forks

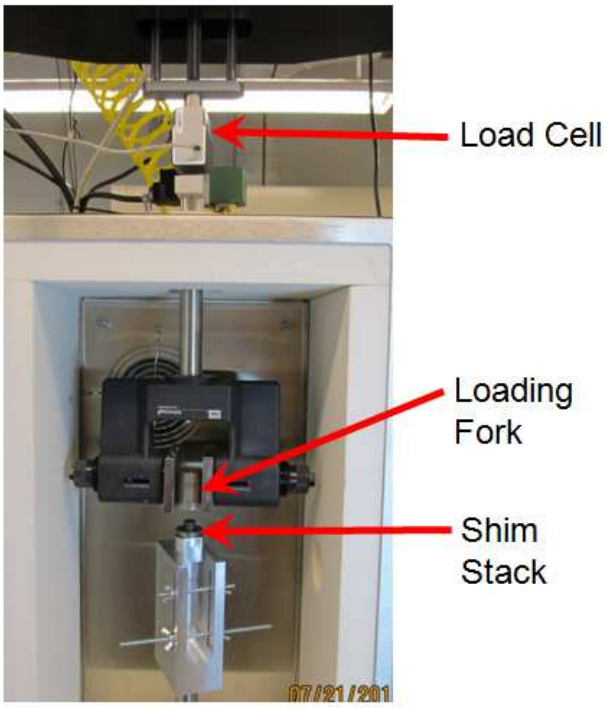

Figure 11: Experimental Setup for Shim Stiffness Characterization

The stiffness of the fixtures used in this experiment is significant. In order to obtain the stiffness of the shims alone, the fixtures and the shims can be modeled as two springs in series. This model is shown in Figure 12. In this model, k_{eff} is the stiffness obtained when the load is applied to the shims while $k_{fixture}$ is the stiffness obtained when the load is applied to the fixtures with the shims removed. Equations

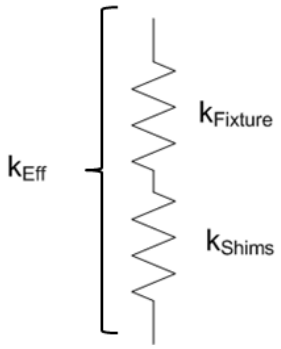

Figure 12: Diagram of Fixtures and Shims in Series

$$k_{eff} = \left(k_{shims}^{-1} + k_{fixture}^{-1}\right)^{-1} \tag{29}$$

$$k_{shims} = \left(k_{eff}^{-1} - k_{fixture}^{-1}\right)^{-1} \tag{30}$$

Preliminary shim stiffness testing showed that the stiffness curve contained three regions. These three regions can be seen in Figure 15. The first region is an extremely nonlinear region. This region is caused by slight misalignment between the shims and the loading fork. Because of this misalignment the prongs of the loading fork do not all contact the shim simultaneously. The effective stiffness changes at each instant that a prong comes into contact with the shim. For this reason region 1 is extremely nonlinear.

The second region begins when the entire loading fork has made contact with the shim. This is the region desired for obtaining the shims stiffness.

The third region occurs when the perimeter of the shim comes into contact with the rigid base. In region three the shim's effective stiffness increases drastically. In some cases the stiffness of region three is infinite indicating that the shim has become effectively rigid. The causes of the three regions of the shim stiffness curve are illustrated in Figure 13.

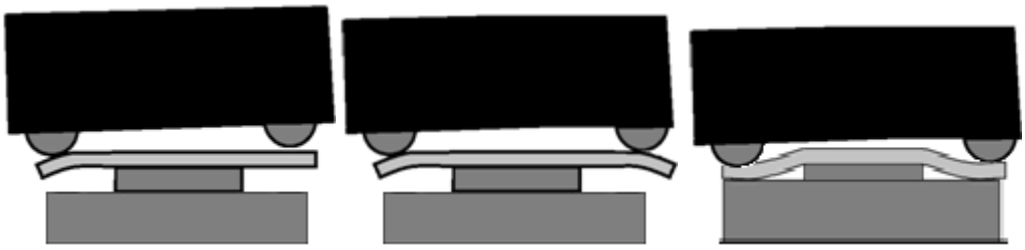

Figure 13: Three Regions of Shim Stiffness Curve

Identifying region two of the stiffness curve was difficult in some cases. For each valve the shim stiffness test was conducted three times for three different shim setups for the purpose of distinguishing region two from the other regions. The first test that was conducted measured the stiffness of the fixtures with the shims removed. This facilitated the identification of region one which is present with or without the shims. The second test that was conducted measured the stiffness of the standard shim setup. The third test that was conducted measured the shim setup with an additional shim inserted as a spacer between the bottom shim and the rigid base. This spacer caused region three to occur only at higher loads. The effect of the spacer is illustrated in Figure 14. When the results of these three tests are plotted together the boundaries of the three regions become much easier to identify.

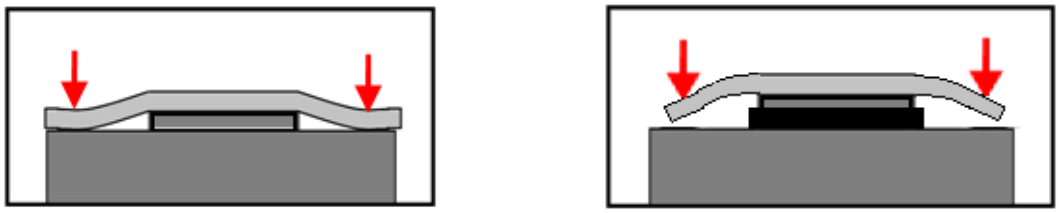

Figure 14: Effect of Spacer Inserted Below Bottom Shim

4.2.2: SZA Valve 1 Results

Figure 15 shows the results of the three tests for SZA valve 1. The stiffness curve of the standard shim setup is shown in Figure 16 with a first order polynomial trend of regions two and three. The slope of the trend line is equal to the stiffness of the shim for each region. Figure 17 shows the stiffness curve of the fixtures alone. Equations 31-32 show the calculation of the isolated shim stiffness for regions two and three.

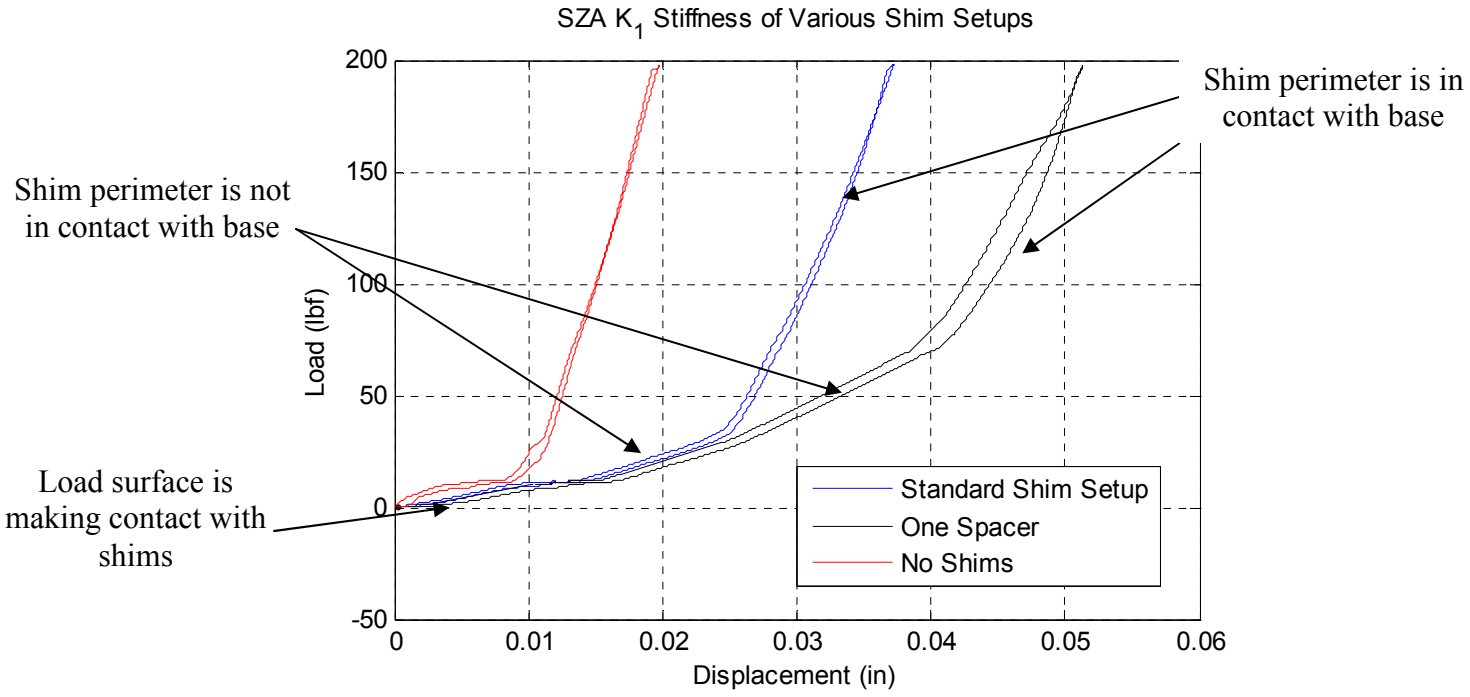

Figure 15: SZA Valve 1 Stiffness of Various Shim Setups

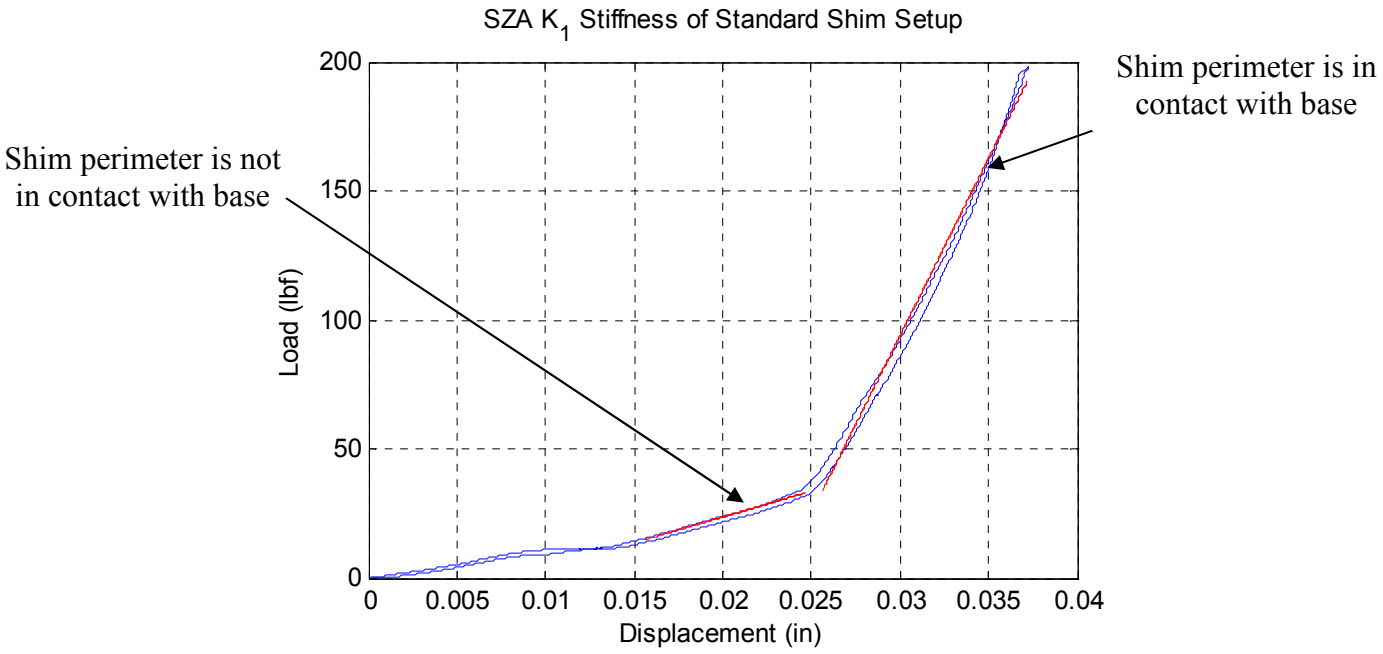

Figure 16: SZA Valve 1 Effective Stiffness of Standard Shim Setup

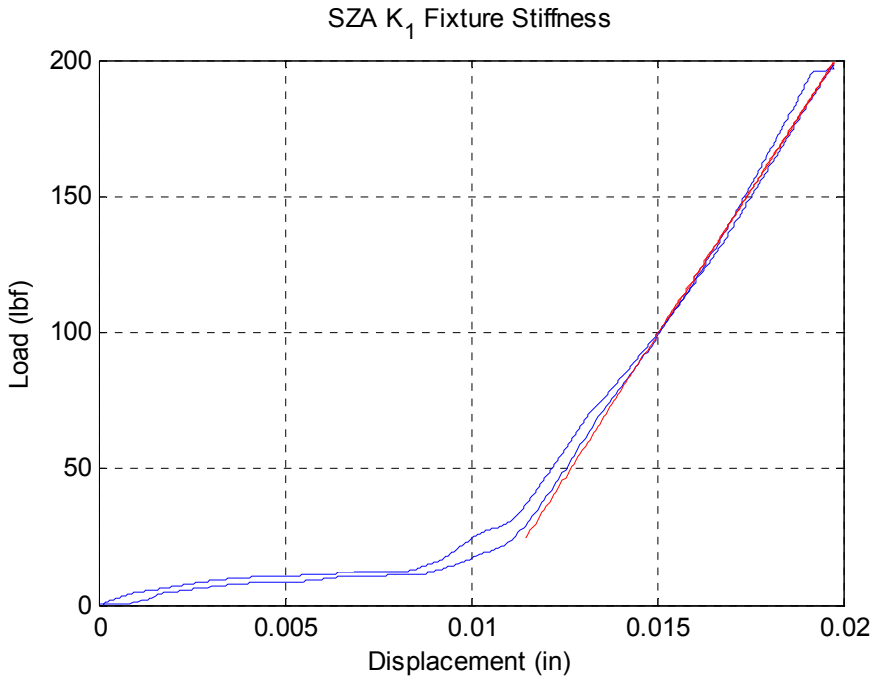

Figure 17: SZA Valve 1 Fixture Stiffness

Shim Stiffness Region 2: No contact exists between shims and base

$$k_{eff} = 2007.6\ lb/in \qquad k_{fixtures} = 21090.8\ lb/in$$

Substituting into Eq. (30)

$$k_{1\ Region\ 2} = (2007.6^{-1} - 21090.8^{-1})^{-1} = 2218.8\frac{lbf}{in} \tag{31}$$

Shim Stiffness Region 3: Contact exists between shims and base

$$k_{eff} = 13729.0\ lb/in \qquad k_{fixtures} = 21090.8\ lb/in$$

Substituting into Eq. (30)

$$k_{1\ Region\ 3} = (13729.0^{-1} - 21090.8^{-1})^{-1} = 39331.8\frac{lbf}{in} \tag{32}$$

$$k_1 = \begin{cases} 388571.4\ N/m\ \ (2218.8\ lbf/in)\ , & F < 151.15\ N\ (33.98\ lbf) \\ 6888053.7\ N/m\ (39331.8\ \ lbf/in), & F \geq 151.15\ N\ (33.98\ lbf) \end{cases}$$

4.2.3: SZA Valve 2 Results

SZA Valve 2, the valve controlling flow of oil from chamber 1 to chamber 2 is unique from the other SZA valves tested in that its shims can absorb much higher loads before making contact with the base. For this reason the valve 2 shims never made contact with the rigid base during testing and only two regions are seen. Figure 18 shows the fixture and shim stiffness. Figure 19 and Figure 20 show these two stiffness curves as well as linear polynomial trends of each curve.

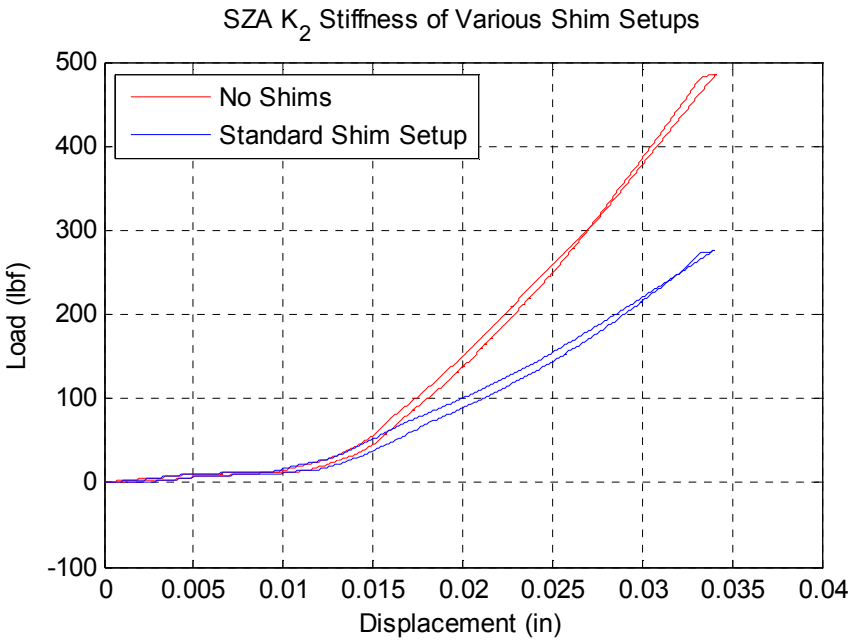

Figure 18: SZA Valve 2 Stiffness of Various Shim Setups

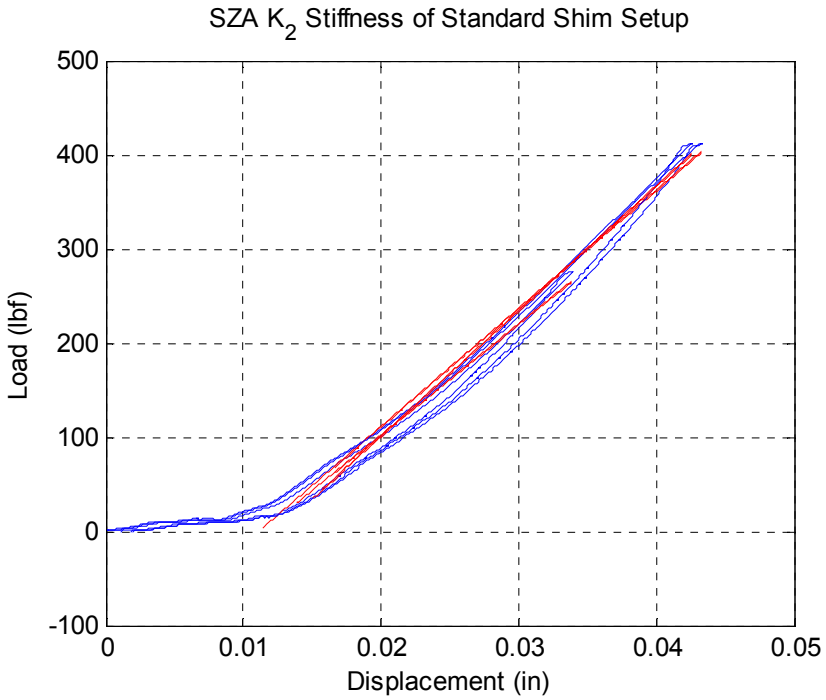

Figure 19: SZA Valve 2 Stiffness of Standard Shim Setup

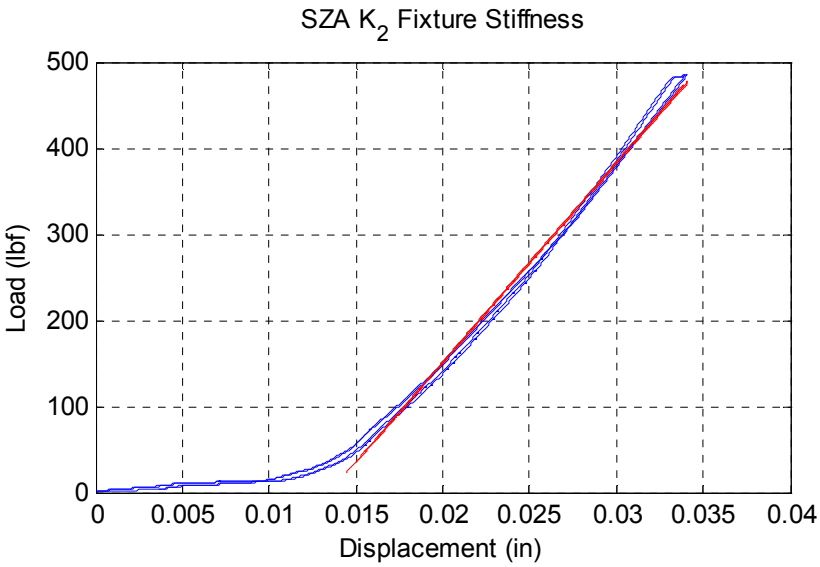

Figure 20: SZA Valve 2 Fixture Stiffness

$$k_{eff} = 893.73\ lb/in \qquad k_{fixtures} = 1690.3\ lb/in$$

Substituting into Eq. (30)

$$k_2 = (893.73^{-1} - 1690.3^{-1})^{-1} = 4790738.2\ N/m\ (27355.82\ lbf/in) \qquad (33)$$

4.2.4: SZA Valve 3 Results

Unlike the other valves tested in this study, valve 3 does not have a rigid backing to restrict the deflection of the shim. Thus the valve 3 shims do not exhibit the same three regions as the other valves. The results of the stiffness tests for this valve implied that the shims did show several distinct regions. However, these regions are a result of nonlinearities in the fixture stiffness curve. This was concluded because the nonlinearities of the fixture stiffness curve occurred at the same loads as the nonlinearities of the shim stiffness curve. These curves are plotted together in Figure 21. Region one is similar to region one of the stiffness curves for the other valves in this study. It occurs because the fixtures are not perfectly aligned and therefore

the initial contact between the loading fork and the shim is not instantaneous. The cause of the other regions of this curve is unknown.

The stiffness test was performed three times. The results of these tests can be seen in Figure 22. Table 7, Table 8, and Table 9 in appendix A.1 contain the stiffness values obtained in each trial for each region. The average stiffness values for regions 2, 3, and 4 are 7757.5, 7096.9, and 9488.4 lb/in respectively. These stiffness values must be substituted into Equation 30 to determine the stiffness of the valve isolated from the test fixtures. This calculation is shown in Equations 34-36. The results of the fixture stiffness tests are shown in Figure 23. Table 23in appendix A.2 shows the stiffness values obtained for each trial. The average fixture stiffness values obtained for regions 2, 3, and 4 are 15234.6, 14616.2, and 18167.9 lb/in respectively.

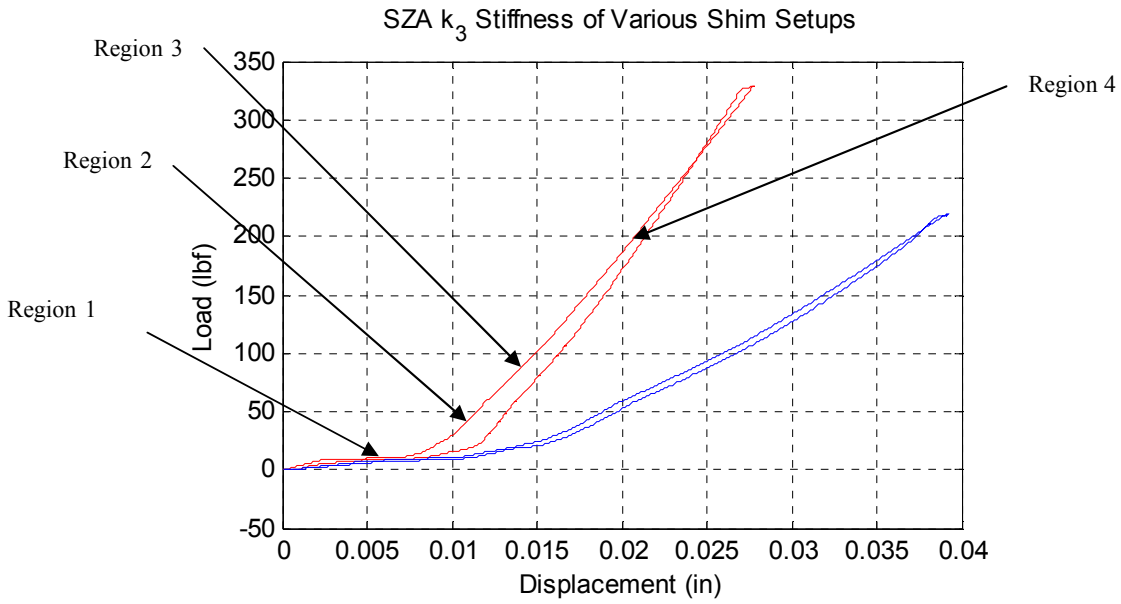

Figure 21: SZA Valve 3Stiffness of Various Shim Setups

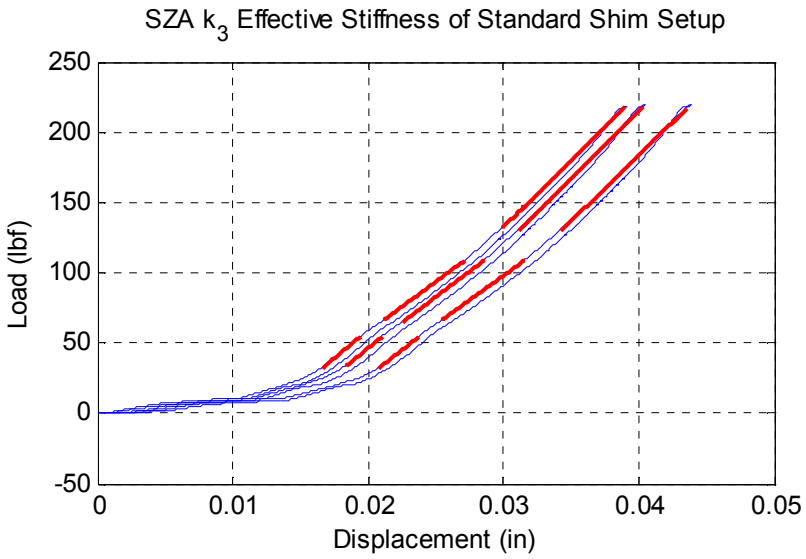

Figure 22: SZA Valve 3 Standard Shim Setup Stiffness

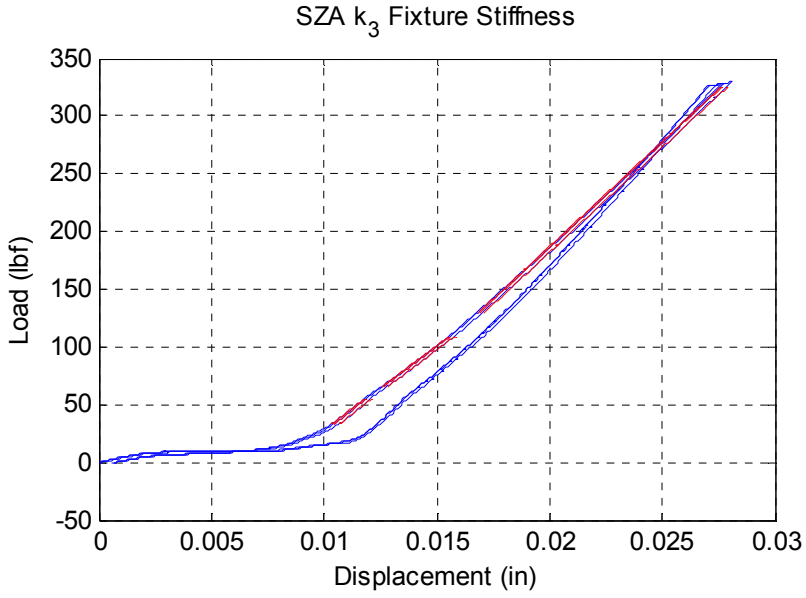

Figure 23: SZA Valve 3 Fixture Stiffness

Shim Stiffness Region 2

$$k_{eff} = 7757.5\ lb/in \qquad k_{fixtures} = 15234.6\ lb/in$$

Substituting into Eq. (30)

$$k_{3\ Region\ 2} = (7757.5^{\ -1} - 15234.6^{-1})^{-1} = 15806.1\ lb/in \tag{34}$$

Shim Stiffness Region 3

$$k_{eff} = 7096.9\ lb/in \qquad k_{fixtures} = 14616.2\ lb/in$$

Substituting into Eq. (30)

$$k_{3\ Reion\ 3} = (7096.9^{-1} - 14616.2^{\ -1})^{-1} = 13795.1\ lb/in \tag{35}$$

Shim Stiffness Region 4

$$k_{eff} = 9488.4\ lb/in \qquad k_{fixtures} = 18167.9\ lb/in$$

Substituting into Eq. (30)

$$k_{3\ Region\ 4} = (\ 9488.4^{\ -1} - 18167.9^{-1})^{-1} = 19861.1\ lb/in \tag{36}$$

$$k_3 = \begin{cases} 2768067.0\ N/m\ (15806.07\ lbf/in), & F < 289.13\ N\ (65\ lbf) \\ 2415894.0\ N/m\ (13795.11\ lbf/in), & 289.13\ N\ (65\ lbf) \le F < 589.27\ N\ (130\ lbf) \\ 3478220.3\ N/m\ (19861.15\ lbf/in), & F \ge 589.27\ N\ (130\ lbf) \end{cases}$$

4.2.5: SZA Valve 4 Results

SZA Valve 4 is subjected to significantly smaller pressure differentials than the other valves. Thus its shims are subjected to smaller loads. For this reason the stiffness of the valve 4 shims is much smaller than that of the other valves. This made stiffness testing difficult because the perimeter of the cantilevered shims would come into contact with the base at very small loads. Because of this region 2 is difficult to distinguish from region 3 using the stiffness curve of the standard shim setup with no spacers.

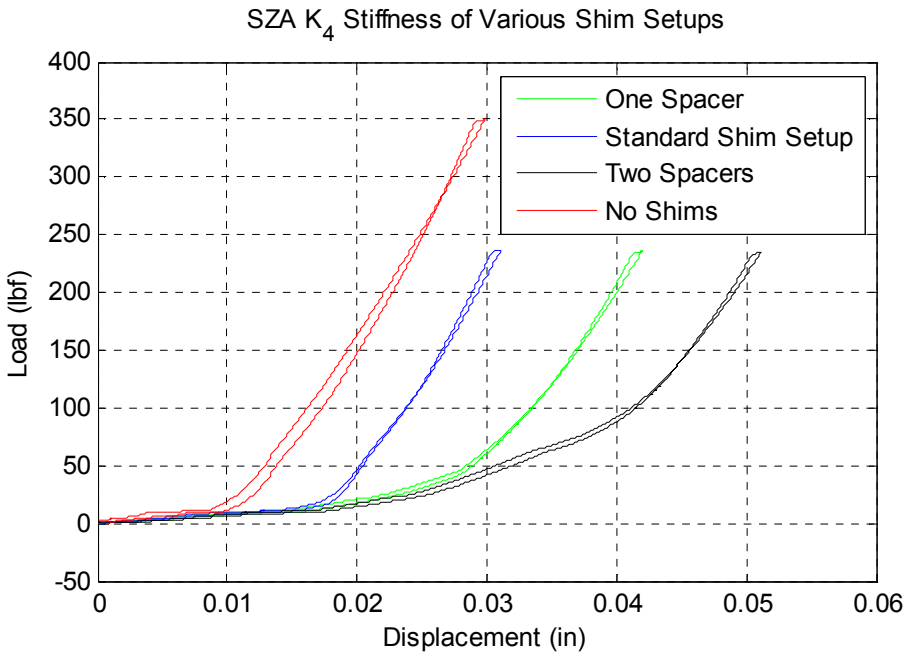

Figure 24: SZA Valve 4 Stiffness of Various Shim Setups

The stiffness curve of the shims with one spacer can be used to determine the stiffness of region 2. The region 2 stiffness of the shims with one spacer is approximately equal to the region 2 stiffness of the standard shim setup in series with the spacer. The spacer that was used was a steel washer with a thickness of 0.012 in. The stiffness of this washer is assumed to be negligible. By using this assumption, the stiffness of region 2 of the standard shim setup can be found by determining the stiffness of region 2 of the shim setup with the spacer. This stiffness is shown in Figure 25.

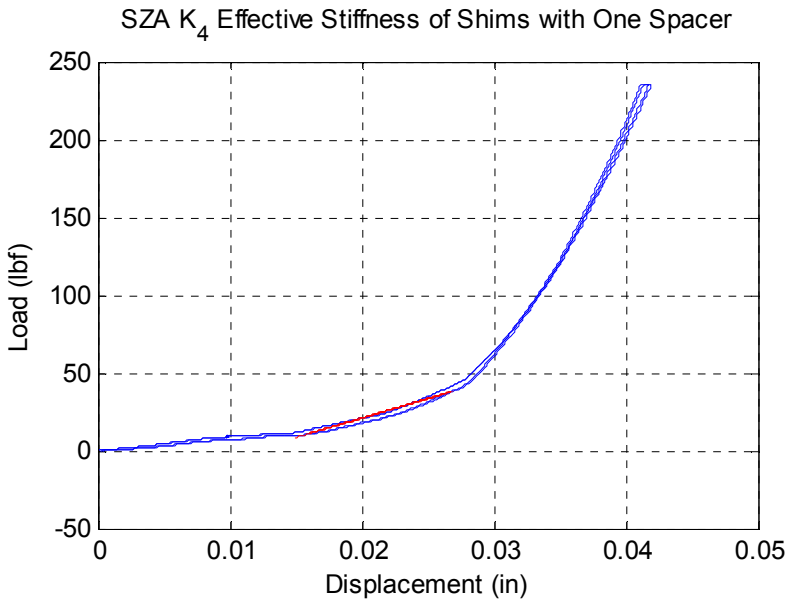

Figure 25: SZA Valve 4 Stiffness of Shim Setup with One Spacer

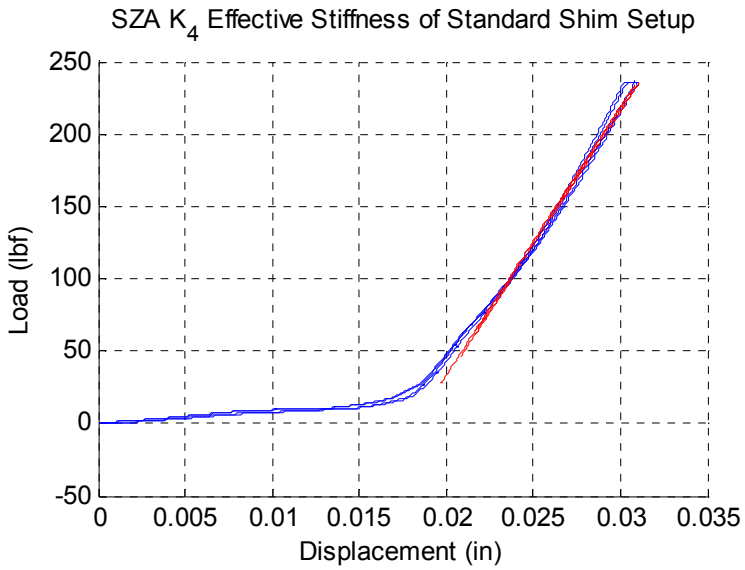

Figure 26: SZA Valve 4 Stiffness of Standard Shim Setup

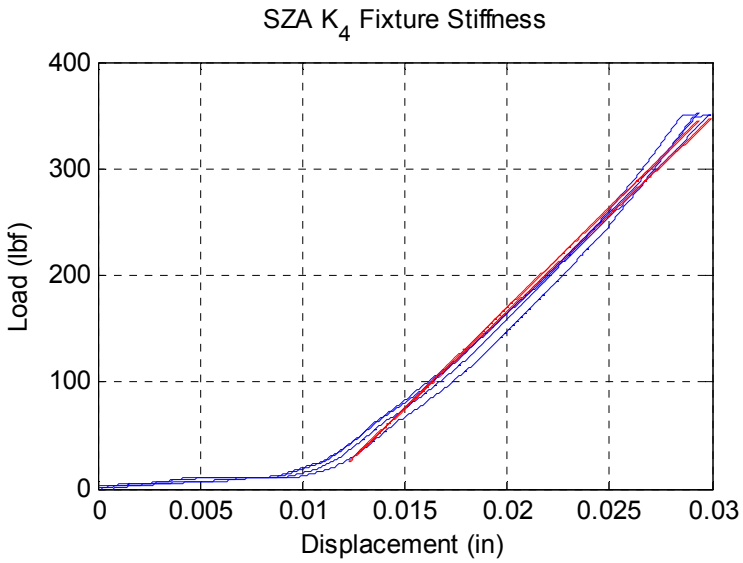

Figure 27: SZA Valve 4 Fixture Stiffness

Shim Stiffness Region 2: No contact exists between shims and base

$$k_{eff} = 2486.4\ lb/in \qquad k_{fixtures} = 18466.4\ lb/in$$

Substituting into Eq. (30)

$$k_{4\ Region\ 2} = (2486.4^{-1} - 18466.4^{-1})^{-1} = 2873.3\ lb/in \tag{37}$$

Shim Stiffness Region 3: Contact exists between shims and base

$$k_{eff} = 18513.7\ lb/in \qquad k_{fixtures} = 18466.4\ lb/in$$

Because k_{eff} is approximately equal to $k_{fixtures}$ the stiffness of the shims can be assumed to be infinite.

$$k_4 = \begin{cases} 503197.2\ N/m \quad (2873.33\ lbf/in), & F < 91.19\ N\ (20.5\ lbf) \\ \infty & F \geq 91.19\ N\ (20.5\ lbf) \end{cases}$$

4.2.6 TK8 Valve 1 Results

Obtaining the stiffness of TK8 valve 1 involved the same difficulties as the SZA 4. The shim bottomed out against the rigid base at such a small load that region 2 of the stiffness curve was indistinguishable from region 1. This problem was overcome, as it was for SZA valve 4, by using the stiffness curve of the shims with one spacer to determine the stiffness of region 2. Figure 28 shows the stiffness curves of the various shim setups.

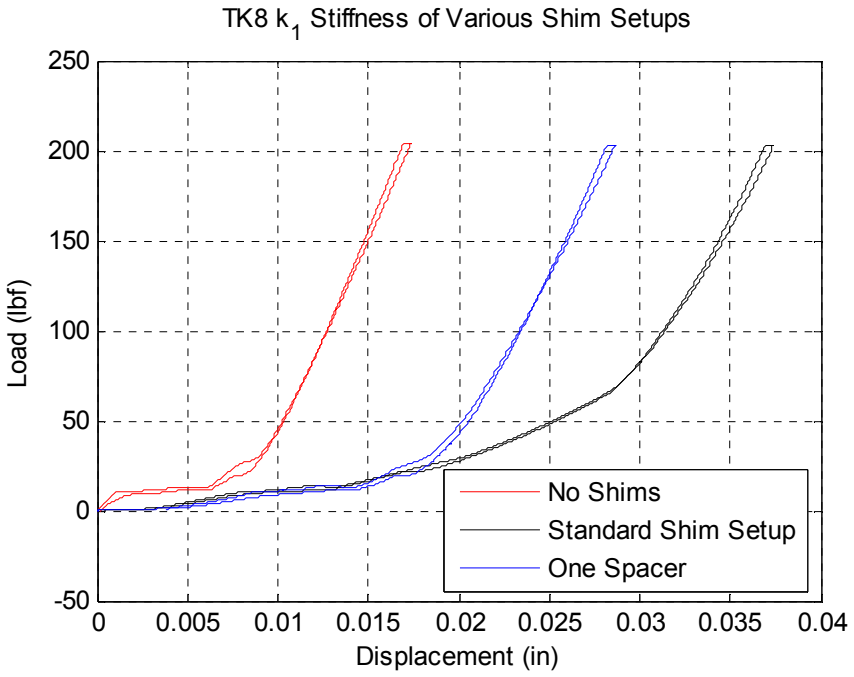

Figure 28: TK8 Valve 1 Stiffness of Various Shim Setups

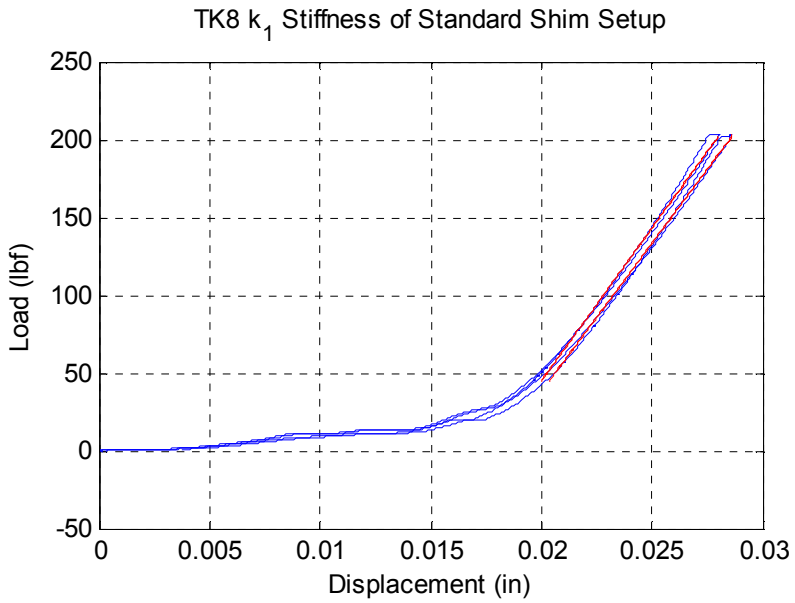

Figure 29: TK8 Valve 1 Stiffness of Standard Shim Setup

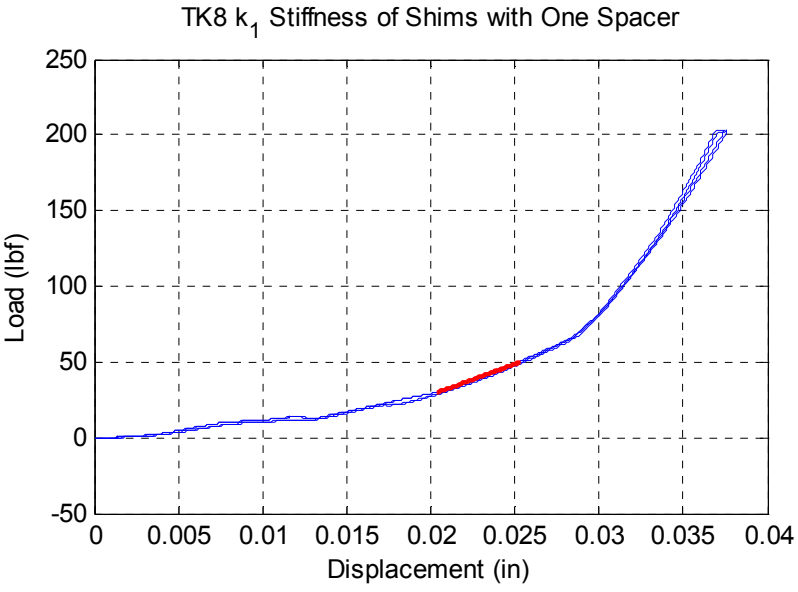

Figure 30: TK8 Valve 1 Stiffness of Shims with One Spacer

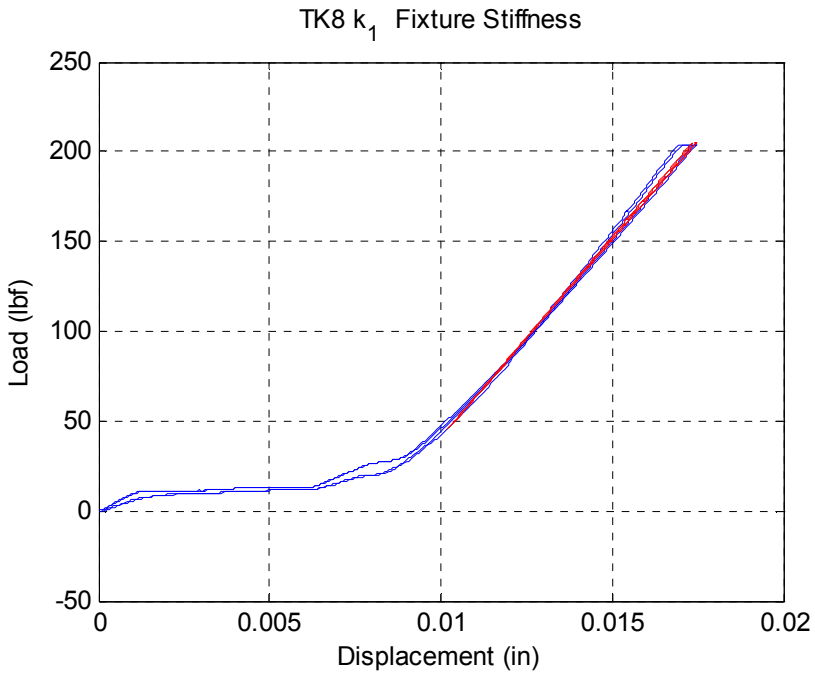

Figure 31: TK8 Valve 1 Fixture Stiffness

Shim Stiffness Region 2: No contact exists between shims and base

$$k_{eff} = 4087.45\ lb/in \qquad k_{fixtures} = 22214.47\ lb/in$$

Substituting into Eq. (30)

$$k_{1\ Region\ 2} = (4087.45^{-1} - 22214.47^{-1})^{-1} = 5009.13 lb/in \tag{38}$$

Shim Stiffness Region 3: Contact exists between shims and base

$$k_{eff} = 19339.73\ lb/in \qquad k_{fixtures} = 22214.47 lb/in$$

Substituting into Eq. (30)

$$k_{1\ Region\ 3} = (19339.73^{-1} - 22214.47^{-1})^{-1} = 149447.20\ lb/in \approx \infty \tag{39}$$

$$k_1 = \begin{cases} 877233.1\ N/m\ (5009.13\ lbf/in), & F < 133.45\ N\ (30\ lbf) \\ \infty, & F \geq 133.45\ N\ (30\ lbf) \end{cases}$$

4.2.7 TK8 Valve 2 Results

The TK8 valve 2 setup has a completely different design than any of the other shims in this study. This valve uses a coil spring in addition to a shim stack to achieve the desired valve stiffness. For this valve, the stiffness was measured using two methods. The first method was to measure the stiffness of the coil spring and the shims separately. The second method was to measure the effective stiffness of the two components together.

The first method of obtaining the stiffness of the TK8 valve 2 shims was to measure the effective stiffness of the two components together. This method is the same method used to determine the on for the other valves. However, the TK8 k_2 curve is unique because its shims never come into contact with a rigid base. Although the shims never contact the base, the TK8 valve 2 stiffness curve appears to be nonlinear as can be seen in Figure 32. Because this nonlinearity also exists in the stiffness curve of the fixtures with the shims removed, it can be assumed that this nonlinearity is caused by the fixtures. The slope was determined for loads above 250 lbf at which the fixture stiffness becomes linear.

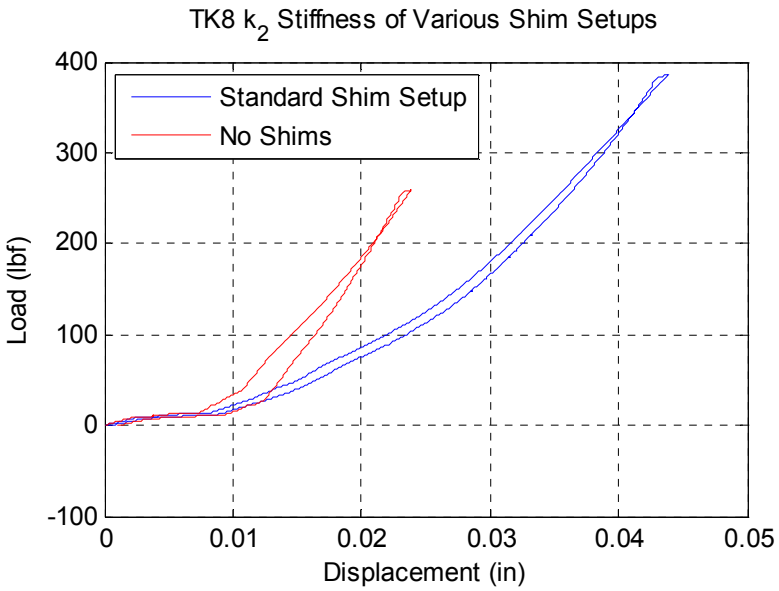

Figure 32: TK8 Valve 2 Stiffness of Various Shim Setups

The stiffness test was performed several times. The results of are shown in Figure 33. Table 14 in appendix A.1contains the stiffness values obtained in each trial. The average stiffness is 1244.3 lb/in. This stiffness must be substituted into Equation 30 to determine the stiffness of the valve isolated from the test fixtures. This calculation is shown in Equation 40. The results of the fixture stiffness tests are shown in Figure 34 and the stiffness values of each test are shown in Table 28 in appendix A.2. The average fixture stiffness is 22490.8 lb/in.

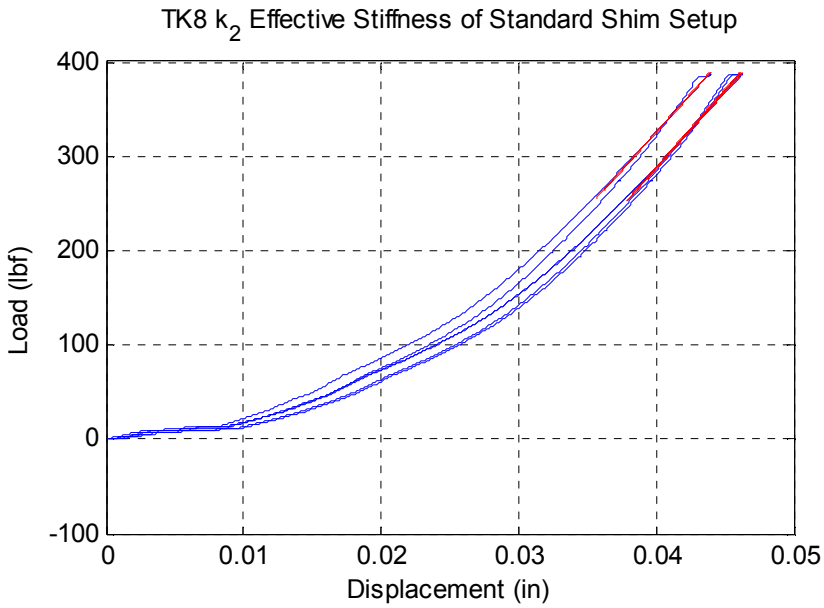

Figure 33: TK8 Valve 2 Standard Setup Stiffness

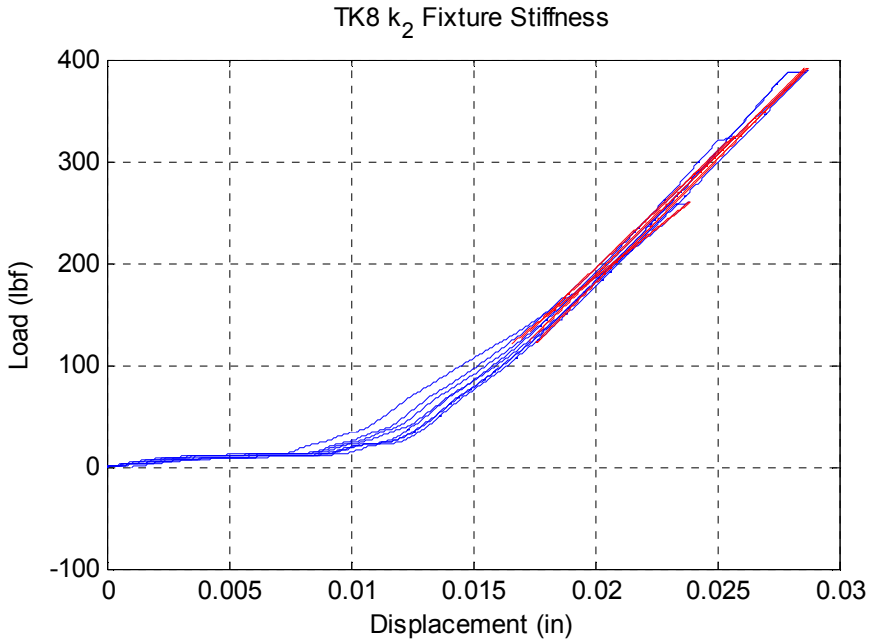

Figure 34: TK8 Valve 2 Fixture Stiffness

$$k_{eff} = 16267.4\, lb/in \qquad k_{fixtures} = 22490.8 lb/in$$

Substituting into Eq. (30)

$$k_2 = (16267.4^{-1} - 22490.8^{-1})^{-1} = 58788.02\ \ lb/in \tag{40}$$

The second method for measuring the stiffness was to measure the stiffness of each component separately. Obtaining the stiffness of each individual component of this valve required that these components be tested separately. Figure 35 - Figure 37 show the test setups used for measuring each component's stiffness. Measuring the stiffness of the coil spring was challenging because it was difficult to apply the load directly to the top of the spring. This challenge was overcome by placing a steel washer over the spring. This washer is assumed to be rigid. The results of the component stiffness tests are shown in Figure 38 and Figure 39. The stiffness values obtained are shown if Table 3.

Figure 35: Standard TK8 Valve 2 Setup

Figure 36: TK8 Valve 2 Setup without Shims

Figure 37: TK8 Valve 2 Setup without Coil Spring

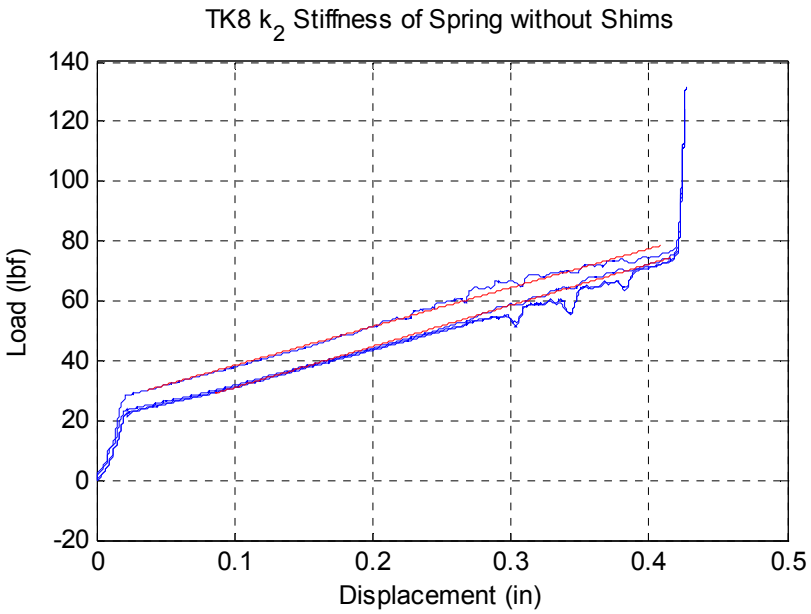

Figure 38: TK8 Valve 2 Coil Spring Stiffness

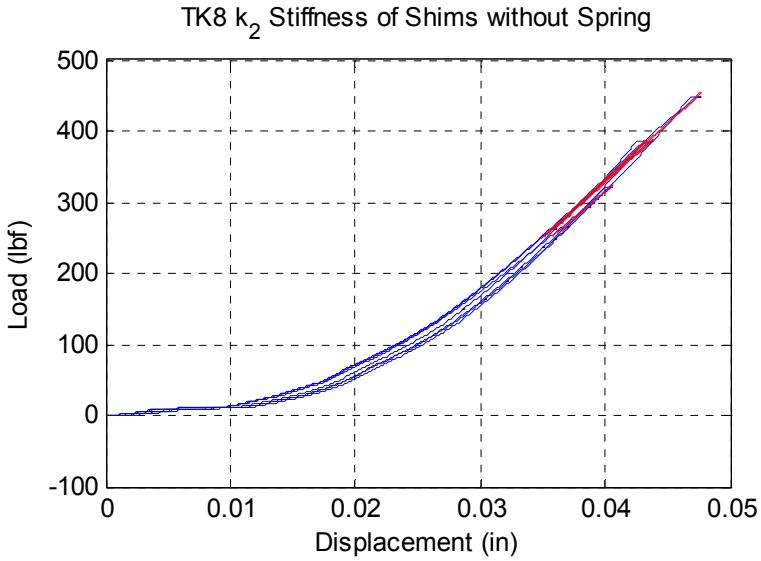

Figure 39: TK8 Valve 2 Shim Stiffness

Table 3: TK8 Valve 2 Shim and Coil Spring Stiffness Values Obtained from Testing

Component	Stiffness Value (lb/in)
Coil Spring	133.98
Shim	15939.3

Each of the stiffness values in Table 3 must be substituted into Equation 30 to obtain the stiffness of these components when isolated from the fixtures. Calculation of the isolated stiffness values is shown in Equations 41-42. The fixture stiffness value is obtained from Figure 34. This value is 22490.8 lb/in.

$$k_{Coil} = (133.98^{-1} - 22490.8^{-1})^{-1} = 134.78\ lb/in \tag{41}$$

$$k_{Shim} = (15939.3^{-1} - 22490.8^{-1})^{-1} = 54718.4\ lb/in \tag{42}$$

The coil spring can be modeled in parallel with the stiffness of the shims. Figure 40 shows a diagram of the shims and coil springs. This diagram also shows the stiffness of the collar on which the shims rest. However, in the calculations this collar is assumed to be rigid. Equation 43 shows the calculation of the effective stiffness of the valve.

$$k_{eq} = k_{coil} + (k_{Shim}^{-1} + k_{Collar}^{-1})^{-1} \tag{43}$$

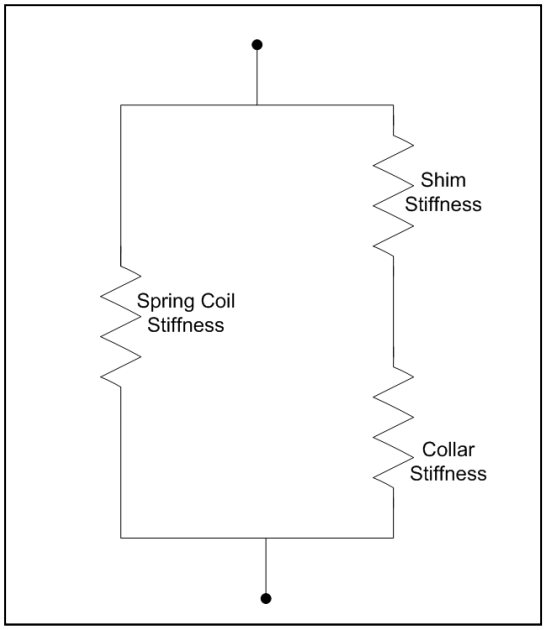

Figure 40: Diagram of TK8 Valve 2 Stiffness

The effective stiffness can be obtained by substituting the stiffness values of the shims and coil spring into Equation 44.

$$k_{eff} = 134.78 + (54718.4^{-1} + \infty^{-1})^{-1} = 54853.2\ lb/in \quad (44)$$

Table 4: TK8 Valve 2 Stiffness Obtained by Various Methods

Method 1 Stiffness (lb/in)	Method 2 Stiffness (lb/in)	Percent Difference %
58788.02	54853.2	6.7

$$k_2 = 10295359.9\ N/m\ (58788.02\ lbf/in)$$

4.2.8 TK8 Valve 3 Results

The TK8 valve 3 shim and fixture stiffness curves are shown in Figure 41. The stiffness curve of TK8 valve 3 was divided into 4 regions similar to the SZA valve 3.

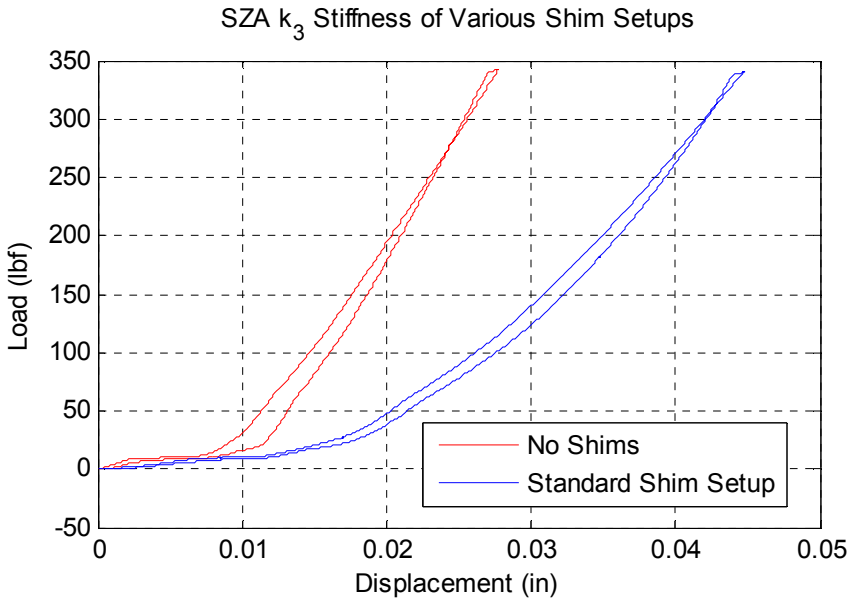

Figure 41: TK8 Valve 3 Stiffness of Various Shim Setups

The stiffness test was performed three times. The results of these tests can be seen in Figure 42. Table 17, Table 18, and Table 19 in appendix A.1 contain the stiffness values obtained in each trial for each region. The average stiffness for regions 2, 3, and 4 is 8308.0, 8645.4, and 13808.0 lb/in respectively. Theses stiffness must be substituted into Equation 30 to determine the stiffness of the valve isolated from the test fixtures. This calculation is shown in Equations 45-47. The results of the fixture stiffness tests are shown in Figure 43. Table 29, Table 30, and Table 31 in appendix A.2 shows the stiffness values obtained in each trial for each region. The average fixture stiffness for regions 2, 3, and 4 is 15880.1, 15235.5, and 8937.8 lb/in respectively.

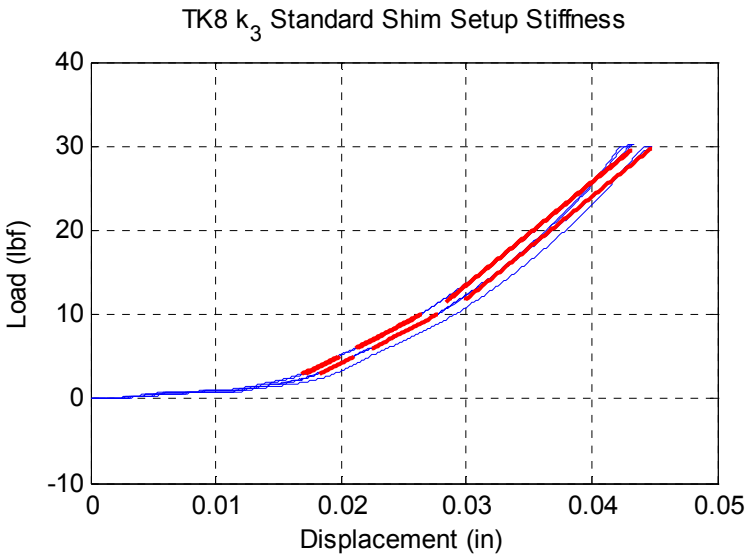

Figure 42: TK8 Valve 3 Standard Shim Setup Stiffness

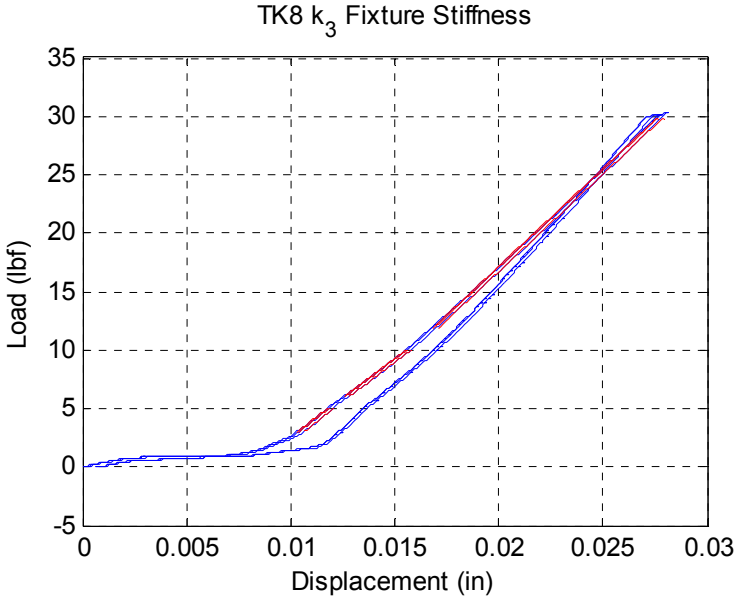

Figure 43: TK8 Valve 3 Fixture Stiffness

Shim Stiffness Region 2

$$k_{eff} = 8308.0\ lb/in \qquad k_{fixtures} = 15880.1\ lb/in$$

Substituting into Eq. (30)

$$k_{3\ Region\ 2} = (8308.0\ ^{-1} - 15880.1^{-1})^{-1} = 17432.6\ lb/in \quad (45)$$

Shim Stiffness Region 3

$$k_{eff} = 8645.4\ lb/in \qquad k_{fixtures} = 15235.5\ lb/in$$

Substituting into Eq. (30)

$$k_{3\ Region\ 3} = (8645.4^{-1} - 15235.5\ ^{-1})^{-1} = 19987.1\ lb/in \quad (46)$$

Shim Stiffness Region 4

$$k_{eff} = 13808.0\ lb/in \qquad k_{fixtures} = 18937.8\ lb/in$$

Substituting into Eq. (30)

$$k_{3\ Region\ 4} = (\ 13808.0^{-1} - 18937.8^{-1})^{-1} = 50975.8\ lb/in \quad (47)$$

$$k_3 = \begin{cases} 3051334.7\ N/m (17423.57\ lbf/in), & F < 301.14\ N\ (67.7\ lbf) \\ 3500270.6\ N/m\ \ (19987.06\ lbf/in), & 301.14\ N\ (67.7\ lbf) \le F < 569.37\ N\ (128\ lbf) \\ 8927237.5\ N/m\ \ \ (50975.84\ lbf/in), & F \ge 569.37\ N\ (128\ lbf) \end{cases}$$

4.2.9 TK8 Valve 4 Results

Similar to SZA valve 4, TK8 Valve 4 is subjected to significantly smaller pressure differentials than the other valves. Therefore its shims are subjected to smaller loads. For this reason the stiffness of the valve 4 shims is much smaller than that of the other valves. This made stiffness testing difficult because the perimeter of the cantilevered shims would come into contact with the base at very small loads. Because of this region 2 is difficult to distinguish from region 3 on the stiffness curve of the standard shim setup seen in Figure 44.

The solution to this problem is to use the same method used to determine the stiffness of SZA k_4. This was to use the stiffness curve of the shims with one spacer to determine the stiffness of region 2. The spacer that was used was a steel washer with a thickness of 0.012 in. The stiffness of this washer is assumed to be negligible. By using this assumption, the stiffness of region 2 of the standard shim setup can be found by determining the stiffness of region 2 of the shim setup with the spacer. This stiffness curve can be seen in Figure 45. The stiffness of region 2 of this curve is 2071.7 lb/in.

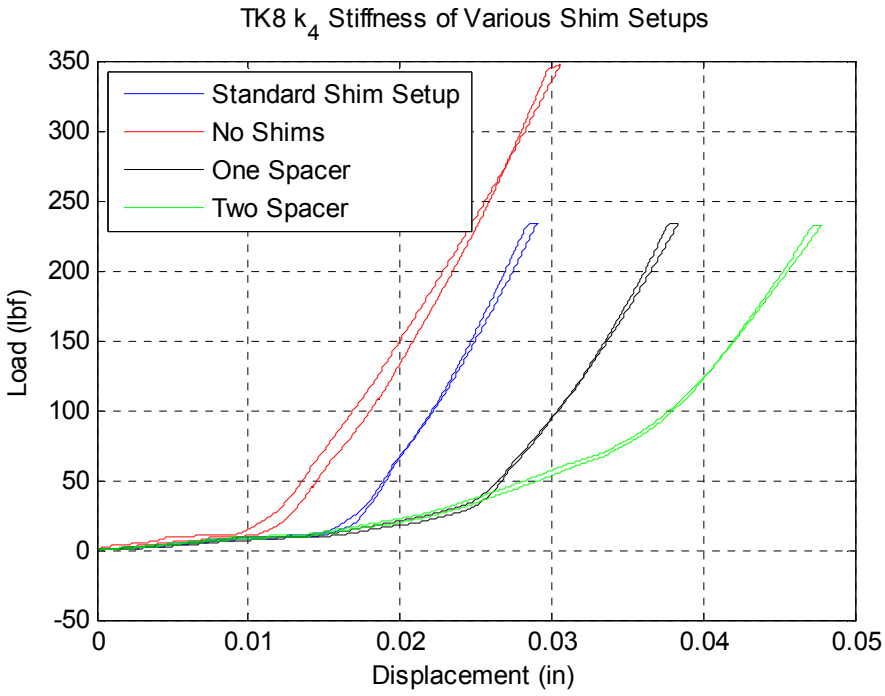

Figure 44: TK8 Valve 4 Stiffness of Various Shim Setups

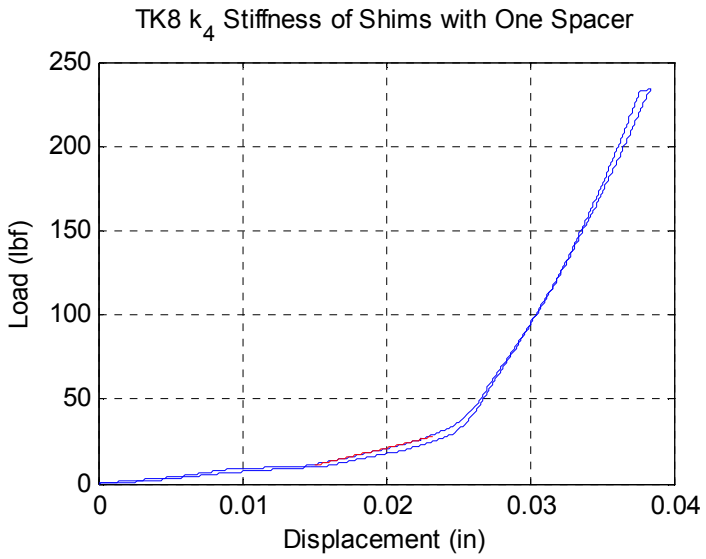

Figure 45: TK8 Valve 4 Stiffness of Shims with One Spacer

The stiffness of region 3 can be determined from the stiffness curve of the standard shim setup shown in Figure 46. The stiffness obtained is 2071.7 lb/in.

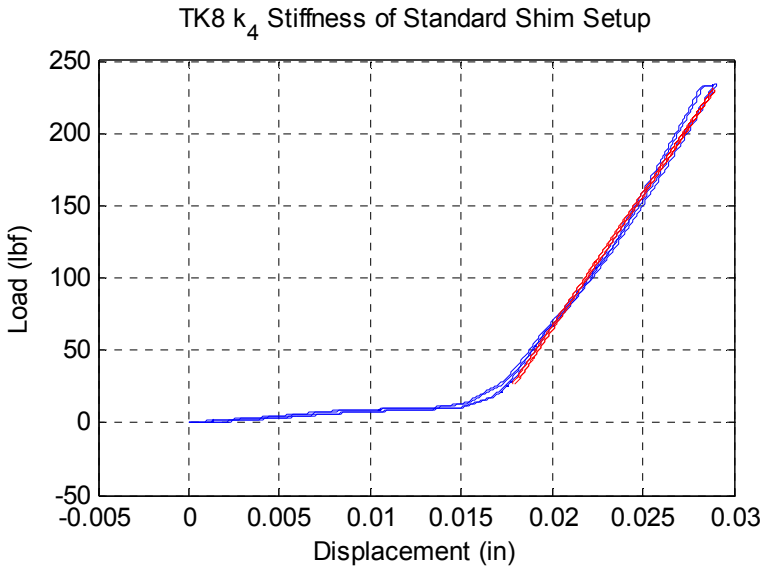

Figure 46: TK8 Valve 4 Standard Shim Setup

The stiffness curve of the TK8 k_4 fixtures is shown in Figure 47. The average stiffness of the fixtures is 18523.7lb/in. Equation 48 shows the calculation of the valve stiffness isolated from the fixtures.

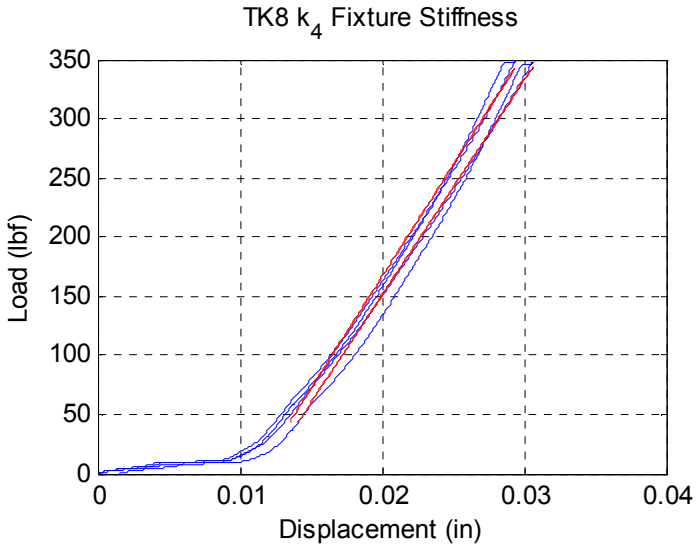

Figure 47: TK8 Valve 4 Fixture Stiffness

Shim Stiffness Region 2: No contact exists between shims and base

$$k_{eff} = 2071.7\ lb/in \qquad k_{fixtures} = 18523.7 lb/in$$

Substituting into Eq. (30)

$$k_{4\ Region\ 2} = (2071.7^{-1} - 18523.7^{-1})^{-1} = 2332.5\ lb/in \tag{48}$$

Shim Stiffness Region 3: Contact exists between shims and base

$$k_{eff} = 18497.0\ lb/in \qquad k_{fixtures} = 18523.7\ lb/in$$

Because k_{eff} is approximately equal to $k_{fixtures}$ the stiffness of the shims can be assumed to be infinite in region three.

$$k_4 = \begin{cases} 408483.3\ lbf/in\ \ (2332.5\ N/m), & F < 93.4\ N\ (21\ lbf) \\ \infty & F \geq 93.4\ N\ (21\ lbf) \end{cases}$$

CHAPTER 5: BULK MODULUS

5.1 Oil Bulk Modulus

5.1.2 Procedure

Unfortunately, the fluid bulk modulus testing was not able to be conducted inside the damper chamber due to sealing problems. For this reason, a different container is being designed for the fluid bulk modulus test. However, the test procedure will remain the same.

5.2 Gas Bulk Modulus

5.2.1 Background and Theory

Bulk modulus of an ideal gas can be calculated as follows. The equation for bulk modulus is defined in Equation 1. The compliance of an ideal gas is shown in Equation 50. [1]

$$\beta = -V\frac{\Delta P}{\Delta V} \tag{49}$$

For adiabatic compression:

$$C_f = \left[\frac{dV}{dp}\right]_{p=p_0} = \frac{V}{p_0} \tag{50}$$

$$\frac{V}{\left[\frac{dV}{dp}\right]} = p_0 = -\beta \;\rightarrow \beta = -p_0 \tag{51}$$

For isothermal compression:

$$\beta = -k * p_0 \tag{52}$$

$$k_{N_2} = 1.4 \tag{53}$$

$$\beta_{N_2} = -1.4 * p_0 \tag{54}$$

5.2.2 Procedure

The bulk modulus testing was done by compressing the experimental fluid and measuring the fluid pressure at different volumes. For the gas this was able to be done in the damper allowing for an effective bulk modulus to be obtained. This effective bulk modulus includes the bulk modulus of the gas as well as the stiffness of the damper chamber.

Prior to testing, the piston valve shims and reserve valve shims were removed. This setup allowed the initial fluid volume to be the combined volume of chambers 1, 2, and 3. This resulted in a total initial volume of 42.66 in^3. The change in volume was only due to the insertion of the piston rod. When the piston rod is compressed there is an increase in pressure that is partially due to viscous flow through the piston orifices. In order to measure only the increase in pressure due to the compression of the fluid, a static compression was applied until the pressure reached a steady state value. This steady state value was used for the bulk modulus calculations. Equations 55 & 56 were used to determine bulk modulus. A diagram of the setup is shown in Figure 48.

$$\Delta V = A * \Delta d \tag{55}$$

$$\beta = -V \frac{\Delta P}{A * \Delta d} \tag{56}$$

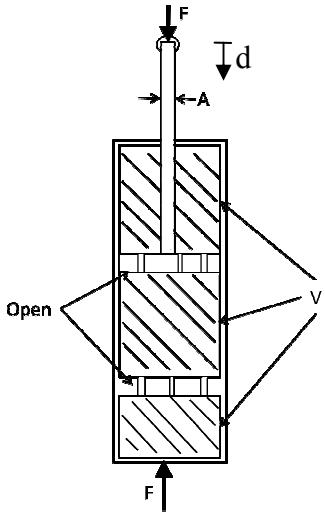

Figure 48: Bulk Modulus Test Setup

The test was performed using a damper dynamometer. This machine was able to apply a known displacement and measure the reaction force of the damper. In order to measure pressure and temperature within the damper, custom chamber accessible dampers were built by Showa R&D. These dampers have a pressure sensor installed in each of the three chambers. The dampers also have a thermocouple installed in chamber 3. The damper used for gas bulk modulus testing is shown in Figure 49.

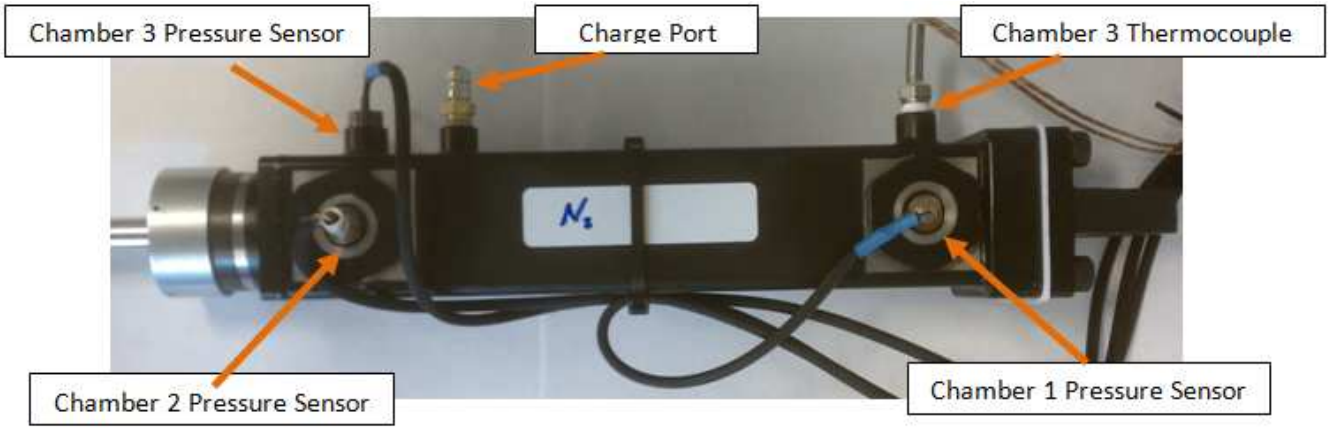

Figure 49: Chamber Accessible Damper

The data was recorded using LabView. A LabView .iv file was created to acquire the three pressure signals, the thermocouple signal, the load cell signal, and the displacement transducer signal. The data was filtered using a low-pass filter with a cutoff frequency of 5 Hz. The block diagram for the LabView setup is shown in Figure 50.

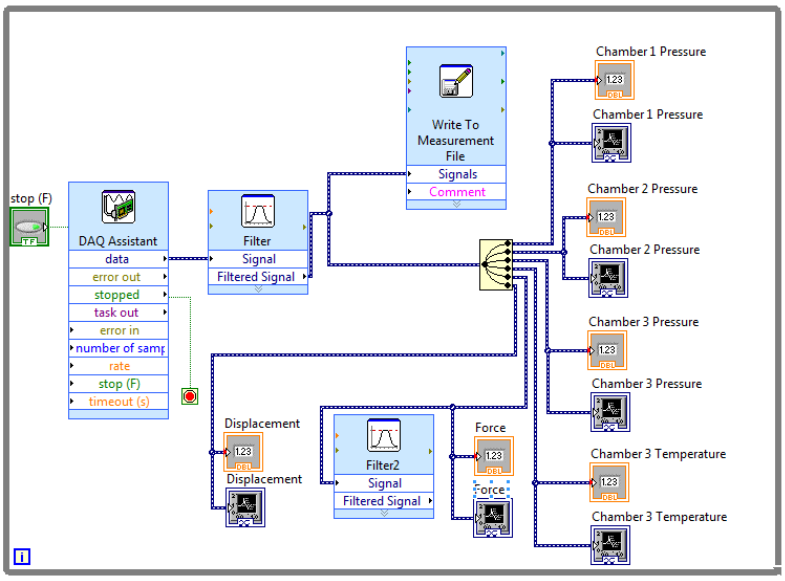

Figure 50: LabView Setup

Twelve tests were conducted to obtain the gas pressure at thirteen volumes. During each test the displacement of the rod started at zero. The rod displacement was then ramped to the desired value where it was held for thirty seconds before returning to zero. The desired displacement started at 10 mm and was increased by 10 mm each test until it reached 120 mm.

5.2.3 Results

Figure 51 shows the chamber volume and steady state pressure for each rod displacement. To obtain the bulk modulus of the fluid the pressure can be plotted against the volumetric strain as shown in Figure 52. Volumetric strain is defined by Equation 57. As seen in Equation 58 the bulk modulus is equal to the negative slope of the pressure versus volumetric

strain plot. The resulting effective bulk modulus at 22 °C and 140.5 psi is shown and compared to the theoretical value in Table 5.

$$\varepsilon_v = \frac{\Delta V}{V_o} \tag{57}$$

$$\beta = -\frac{\Delta P}{\varepsilon_v} \tag{58}$$

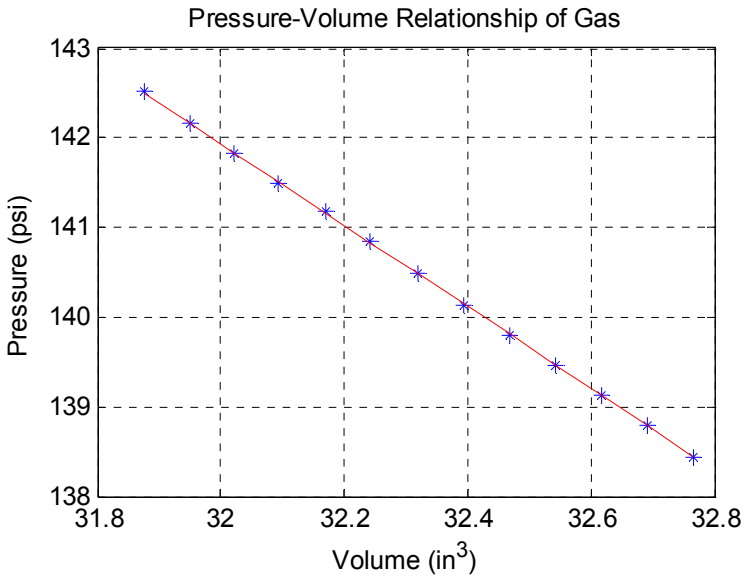

Figure 51: Pressure Volume Relationship of Gas

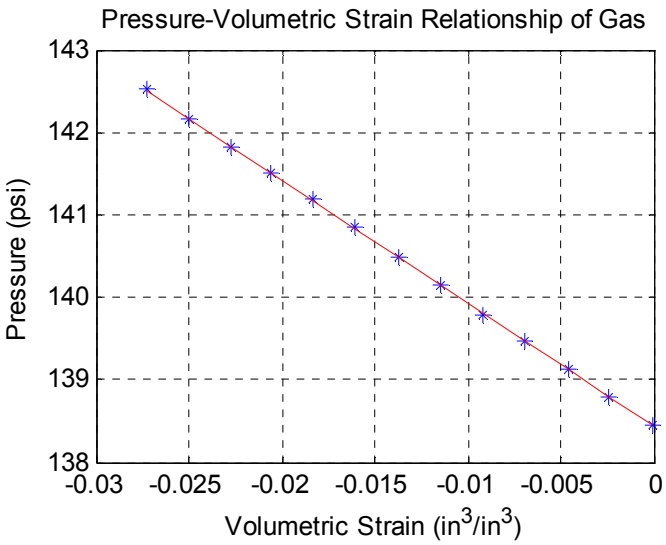

Figure 52: Pressure Volumetric Strain Relationship of Gas

Table 5: Bulk Modulus of Nitrogen Gas at 140.5 psi and 22°C

Method	Value (psi)	Percent Difference (%)
Experimental Bulk Modulus	149.3	-
Theoretical Isothermal Bulk Modulus	196.7	31.7
Theoretical Adiabatic Bulk Modulus	140.5	5.89

BIBLIOGRAPHY

Balasubramanian Karthik Smart Bulk Modulus Sensor [Report] : Masters Thesis. - Gainsville : University of Florida, 2003.

Doebelin Ernest O. System Dynamics: Modeling, Analysis, Simulation, Design [Book]. - New York : Dekker, 1998.

International Organization of Motor Vehicle Manufactures OICA Production Statistics [Online] // OICA.net. - 2011. - August 1, 2011. - http://www.oica.net/category/production-statistics/.

Lang Harold H. A Study of the Characteristics of Automotive Hydraulic Dampers at High Stroking Frequencies [Report] : PhD Thesis. - Ann Arbor : The University of Michigan, 1977.

Lee Ill-Yeong and Sun Dan Dan Evaluation of Effective Bulk Modulus of Oil in Automotive Hyraulic Dampers-Effects of Cylinder Shell Elastic Deformation [Conference] // SICE Annual Conference. - Sapporo : Hokkaido Institute of Technology, 2004. - pp. 2431-2436.

Rhoades Kirk Shawn Development and Experimental Verification of a Parametric Model of an Automotive Damper [Report] : Masters Thesis. - [s.l.] : Texas A&M, 2006.

Shams M. [et al.] CFD-FEA Analysis of Hydraulic Shock Absorber Valve Behavior [Journal] // International Journal of Automotive Technology. - 2007. - pp. 615-622.

Talbott Michael S. and Starkey John An Experimentally Validated Physical Model of a High-Performance Mono-Tube Damper [Journal] // SAE Technical Paper Series. - 2002. - p. 382.

Warren Young C. and Budynas Richard G. Roark's Formulas For Stress And Strain [Book]. - New York : McGraw-Hill, 1989. - 0-07-072542-X.

APPENDIX A: SHIM STIFFNESS

EXPERIMENTAL DATA

A.1 Shim + Fixture Stiffness Tests

Table 6: SZA k_2 Region 2 Fixture + Shim Stiffness Values

Trial	Stiffness
Trial 1	11804.7
Trial 2	12567.3
Trial 3	13298.7
Average	12556.9

Table 7: SZA k_3 Region 2 Fixture + Shim Stiffness Values

Trail	Measured Stiffness (lb/in)
Trial 1	7592.3
Trial 2	7770.9
Trial 3	7909.3
Average	7757.5

Table 8: SZA k_3 Region 3 Fixture + Shim Stiffness Values

Trail	Measured Stiffness (lb/in)
Trial 1	6941.6
Trial 2	7251.9
Trial 3	7097.2
Average	7096.9

Table 9: SZA k_3 Region 4 Fixture + Shim Stiffness Values

Trail	Measured Stiffness (lb/in)
Trial 1	9385.4
Trial 2	9599.6
Trial 3	9480.3
Average	9488.4

Table 10: SZA k_4 Region 2 Fixture + Shim Stiffness

Trail	Measured Stiffness (lb/in)
Trial 1	2478.5
Trial 2	2494.4
Average	2486.4

Table 11: SZA k_4 Region 3 Fixture + Shim Stiffness Values

Trial	Measured Stiffness (lb/in)
Trial 1	18490.0
Trial 2	18537.4
Average	18513.7

Table 12: TK8 k1 Region 2 Fixture + Shim Stiffness Values

Trial	Measured Stiffness (lb/in)
Trial 1	4053.64
Trial 2	4121.26
Average	4087.45

Table 13: TK8 k_1 Region 3 Fixture +Shim Stiffness Values

Trial	Measured Stiffness (lb/in)
Trial 1	19637.27
Trial 2	19042.19
Average	19339.73

Table 14: TK8 k_2 Fixture + Shim Stiffness Values

Trial	Measured Stiffness (lb/in)
Trial 1	16136.3
Trial 2	16514.6
Trial 3	16151.2
Average	16267.4

Table 15: TK8 k_2 Shim + Fixture Stiffness Values without Spring

Trial	Measured Stiffness (lb/in)
Trial 1	15027.4
Trial 2	15782.1
Trial 3	16186.3
Trial 4	16761.5
Average	15939.3

Table 16: TK8 k_2 Coil Spring + Fixture Stiffness Values without Shims

Trial	Measured Stiffness (lb/in)
Trial 1	130.17
Trial 2	137.79
Average	133.98

Table 17: TK8 k_3 Region 2 Fixture + Shim Stiffness Values

Trial	Measured Stiffness (lb/in)
Trial 1	8530.2
Trial 2	8132.4
Trial 3	8261.6
Average	8308.0

Table 18: TK8 k_3 Region 3 Fixture + Shim Stiffness Values

Trial	Measured Stiffness (lb/in)
Trial 1	8746.7
Trial 2	8590.1
Trial 3	8599.4
Average	8645.4

Table 19: TK8 k_3 Region 4 Fixture + Shim Stiffness Values

Trial	Measured Stiffness (lb/in)
Trial 1	13907.7
Trial 2	13784.7
Trial 3	13731.6
Average	13808.0

Table 20: TK8 k_4 Region 2 Fixture + Shim Stiffness Values

Trial	Measured Stiffness (lb/in)
Trial 1	2071.7
Trial 2	N/A
Average	2071.7

Table 21: TK8 k_4 Region 3 Fixture + Shim Stiffness Values

Trial	Measured Stiffness (lb/in)
Trial 1	18520.0
Trial 2	18474.0
Average	18497.0

A.2 Fixture Stiffness Tests

Table 22: SZA k_2 Fixture Stiffness

Trial	Measured Stiffness (lb/in)
Trial 1	23178.3
Trial 2	23244.7
Average	23211.5

Table 23: SZA k_3 Region 2 Fixture Stiffness

Trial	Measured Stiffness (lb/in)
Trial 1	15244.2
Trial 2	15473.4
Trial 3	14975.1
Average	15234.6

Table 24: SZA k_3 Region 3 Fixture Stiffness

Trial	Measured Stiffness (lb/in)
Trial 1	14648.1
Trial 2	14606.8
Trial 3	14593.6
Average	14616.2

Table 25: SZA k_3 Region 4 Fixture Stiffness

Trial	Measured Stiffness (lb/in)
Trial 1	18200.6
Trial 2	18127.2
Trial 3	18175.9
Average	18167.9

Table 26: SZA k_4 Fixture Stiffness

Trial	Measured Stiffness (lb/in)
Trial 1	18206.9
Trial 2	18725.9
Average	18466.4

Table 27: TK8 k_1 Fixture Stiffness

Trial	Measured Stiffness (lb/in)
Trial 1	22015.32
Trial 2	22413.61
Average	22214.47

Table 28: TK8 k_2 Fixture Stiffness

Trial	Measured Stiffness (lb/in)
Trial 1	19081.6
Trial 2	22852.3
Trial 3	23744.5
Trial 4	24285.1
Average	22490.8

Table 29: TK8 k_3 Region 2 Fixture Stiffness

Trial	Measured Stiffness (lb/in)
Trial 1	15901.6
Trial 2	16129.1
Trial 2	15609.7
Average	15880.1

Table 30: TK8 k_3 Region 3 Fixture Stiffness

Trial	Measured Stiffness (lb/in)
Trial 1	15268.8
Trial 2	15225.8
Trial 3	15211.9
Average	15235.5

Table 31: TK8 k_3 Region 4 Fixture Stiffness

Trial	Measured Stiffness (lb/in)
Trial 1	18971.9
Trial 2	18895.3
Trial 3	18946.1
Average	18937.8

Table 32: TK8 k_4 Fixture Stiffness

Trial	Measured Stiffness (lb/in)
Trial 1	18168.8
Trial 2	18878.6
Average	18523.7

APPENDIX B: BULK MODULUS TEST DATA

B.1 Gas Bulk Modulus Data

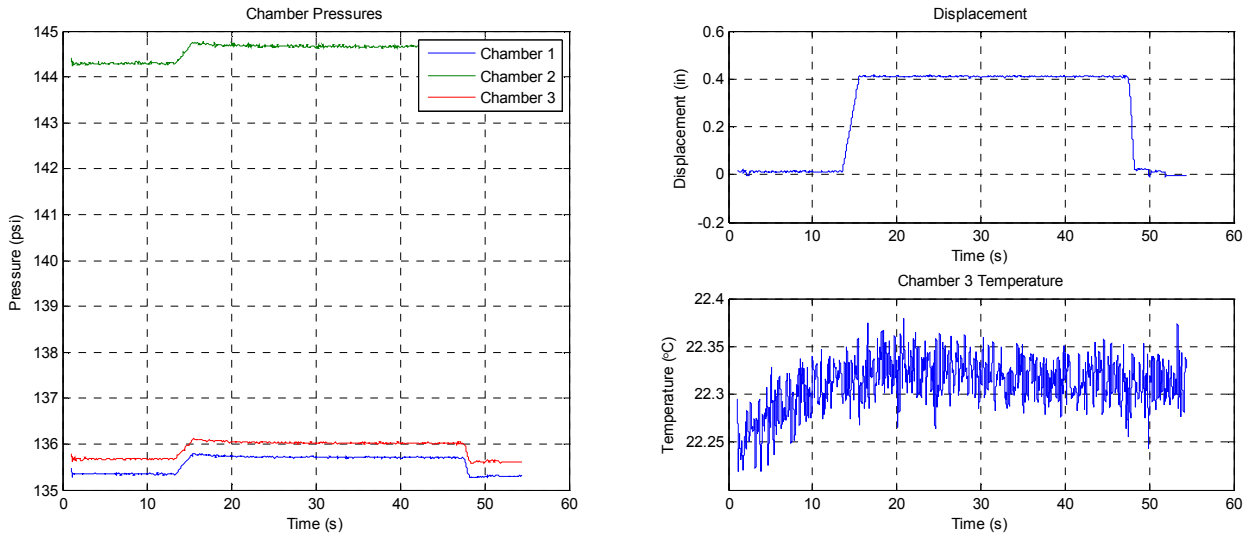

Figure 53: 10 mm Displacement

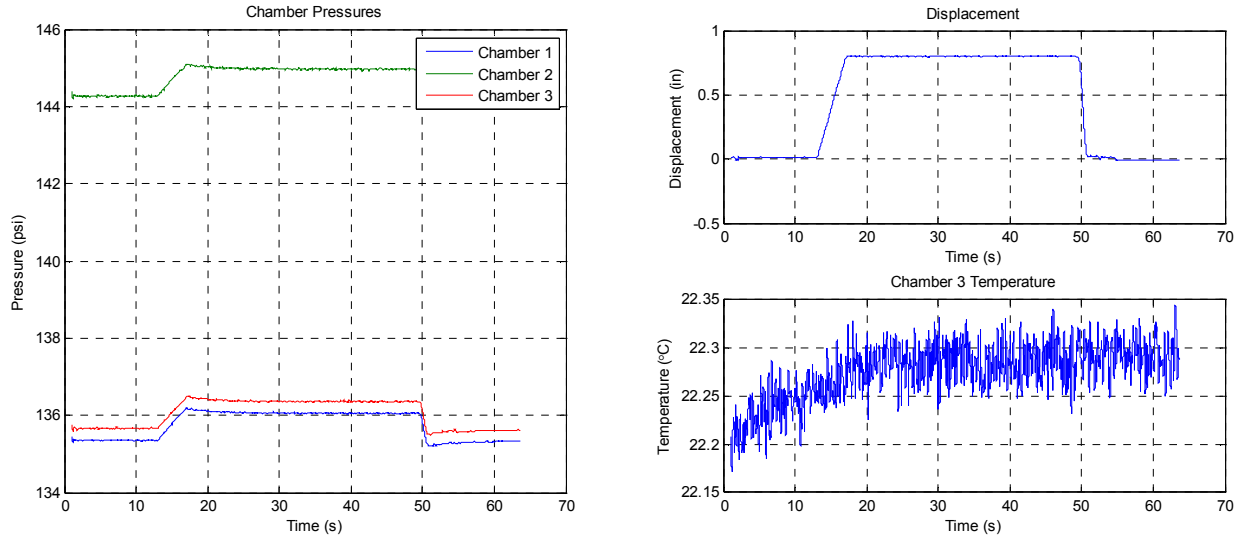

Figure 54: 20 mm Displacement

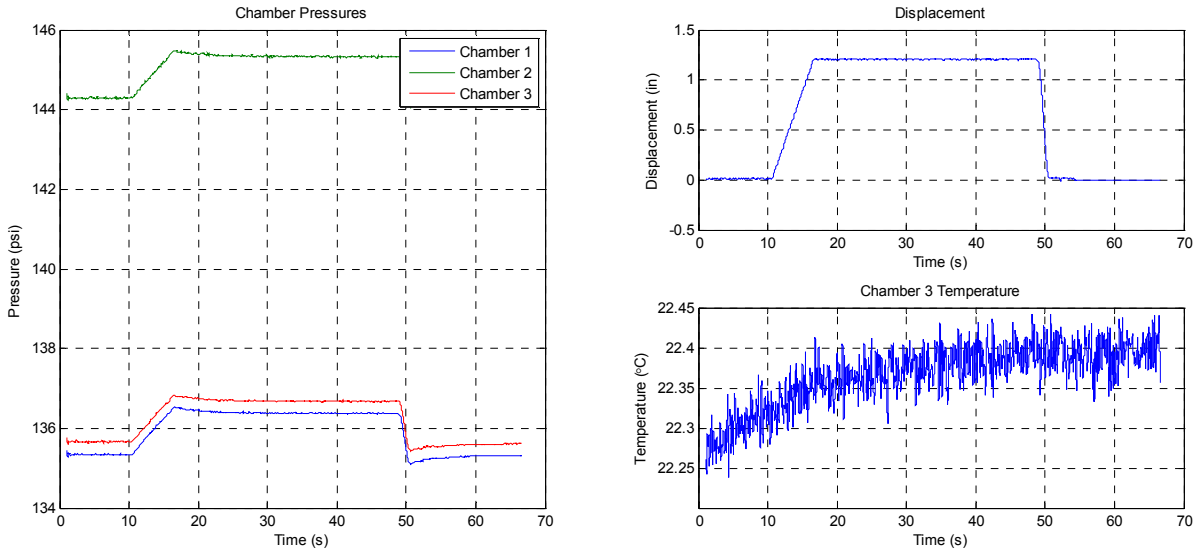

Figure 55: 30 mm Displacement

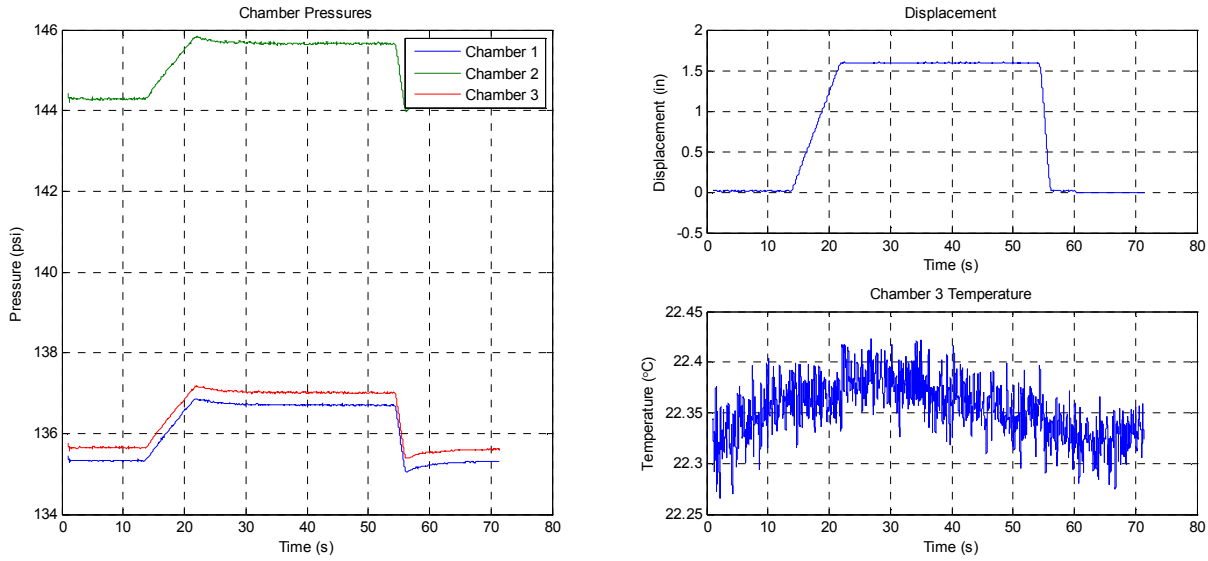

Figure 56: 40 mm Displacement

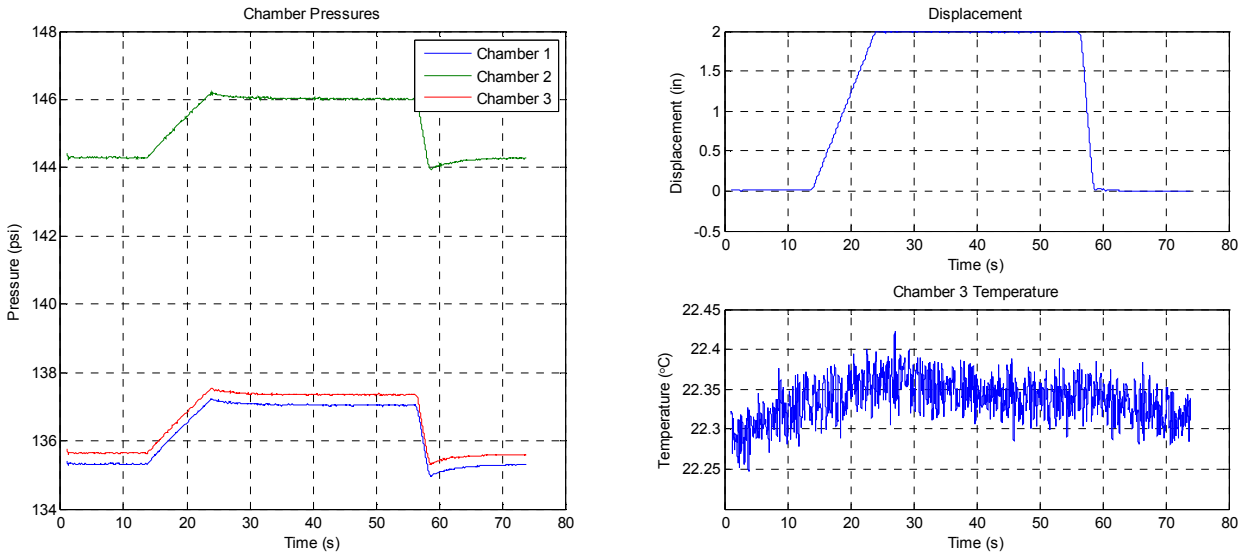

Figure 57: 50 mm Displacement

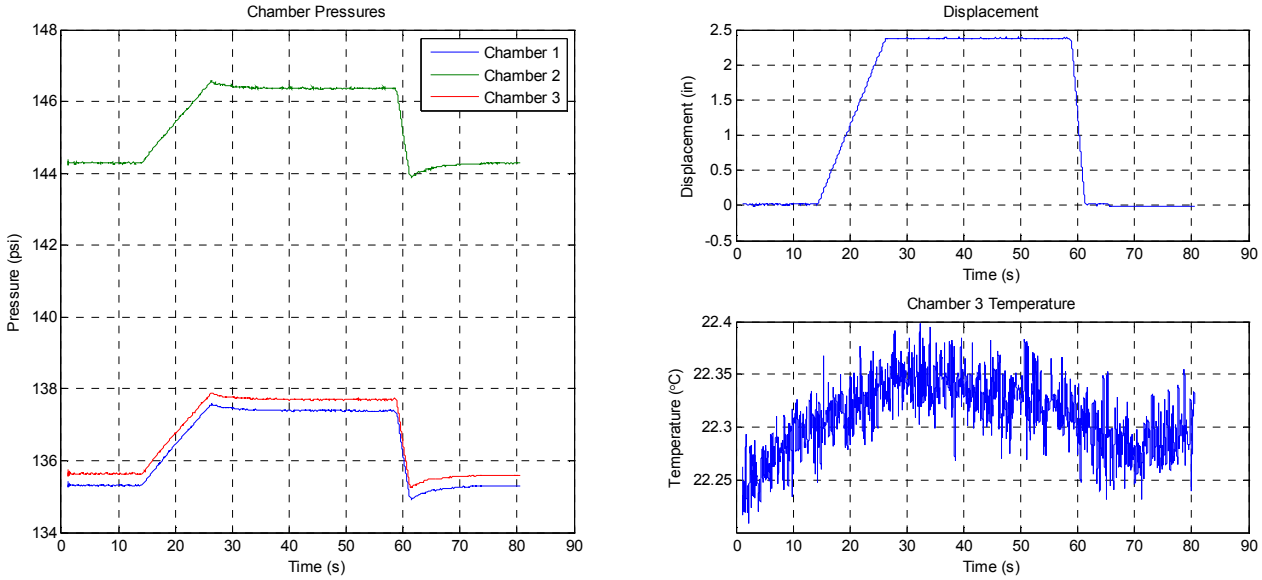

Figure 58: 60 mm Displacement

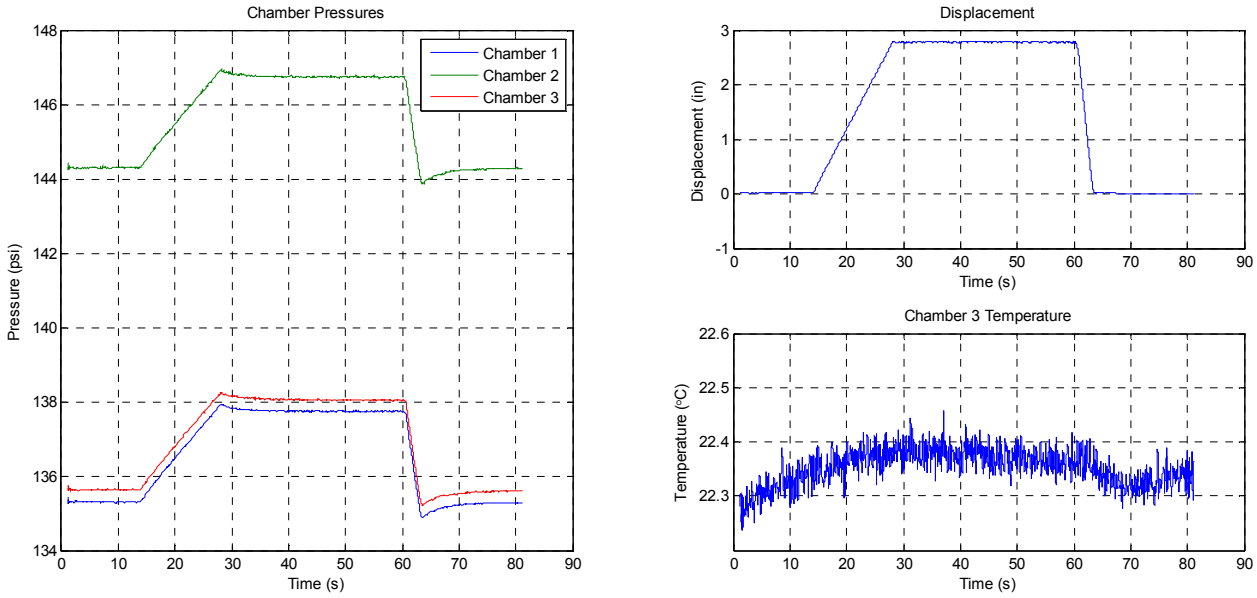

Figure 59: 70 mm Displacement

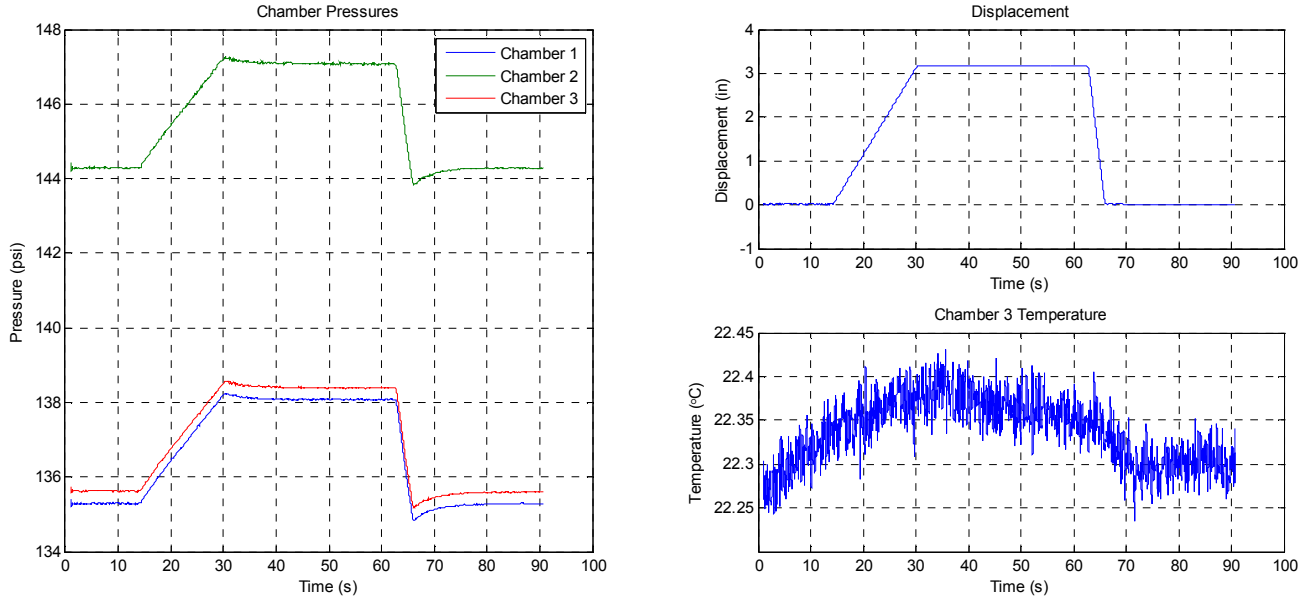

Figure 60: 80 mm Displacement

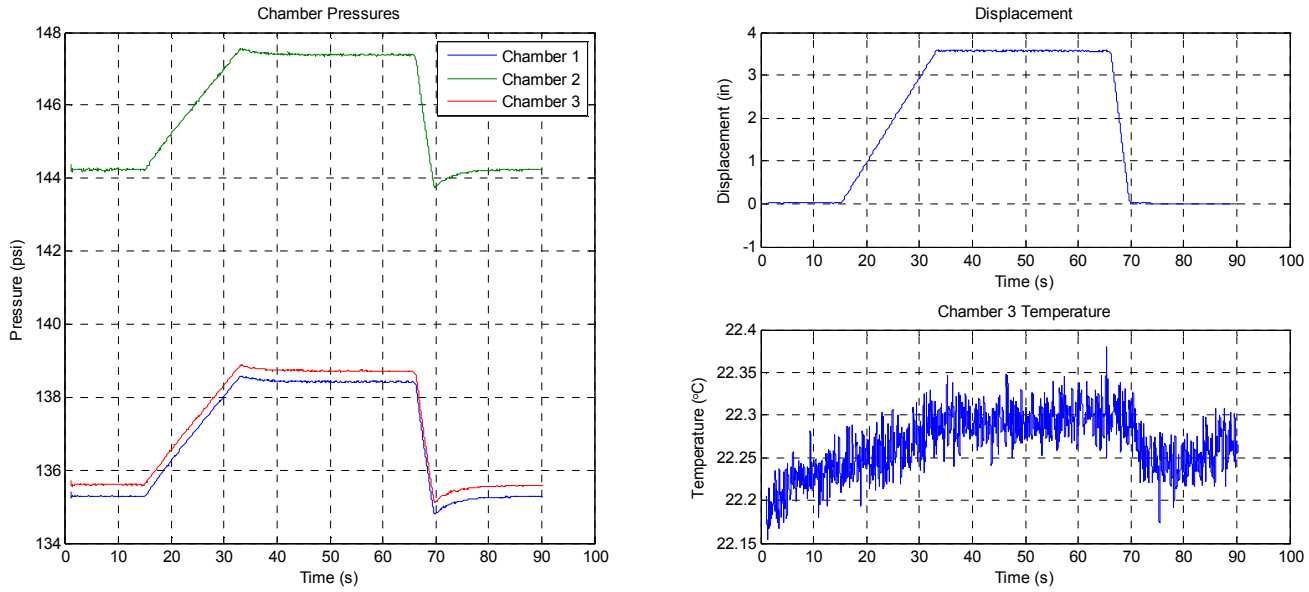

Figure 61: 90 mm Displacement

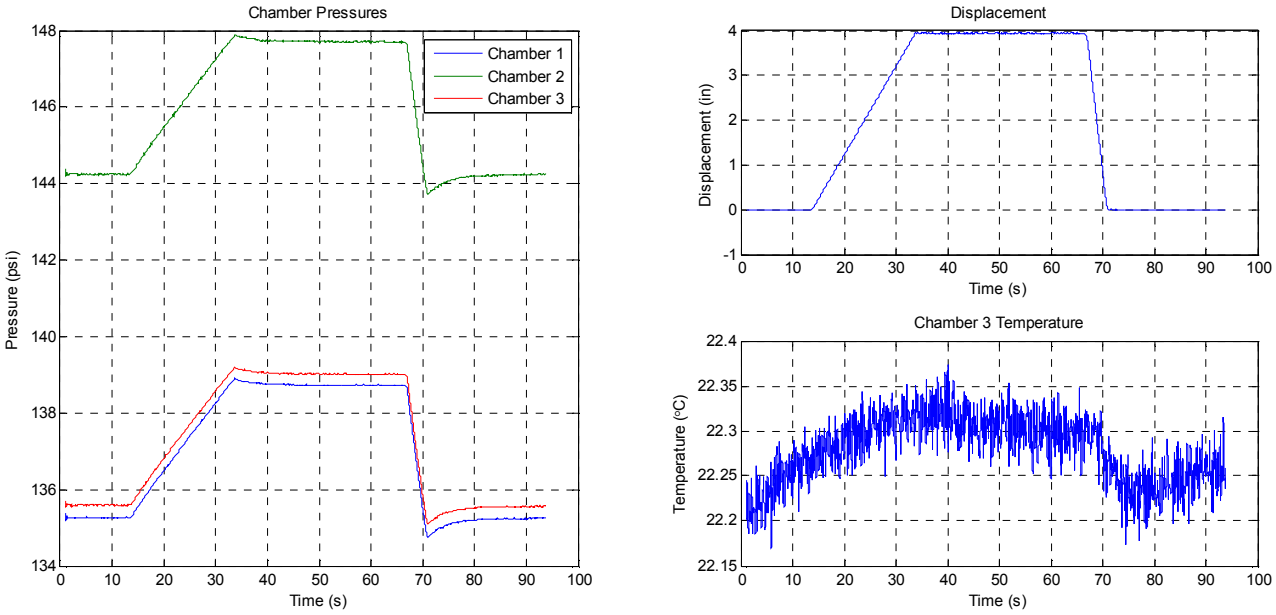

Figure 62: 100 mm Displacement

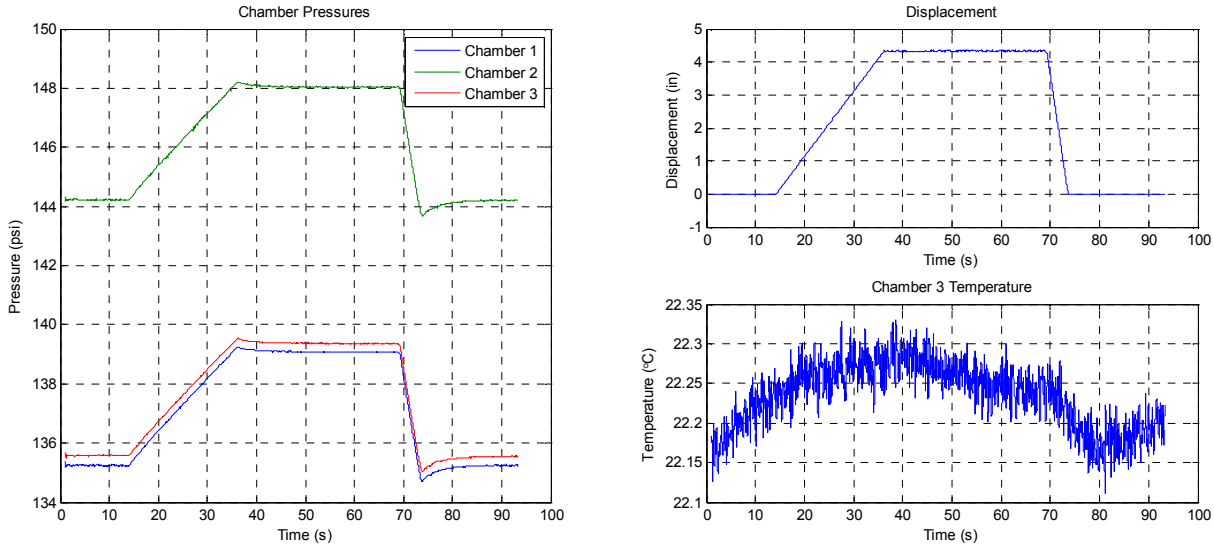

Figure 63: 110 mm Displacement

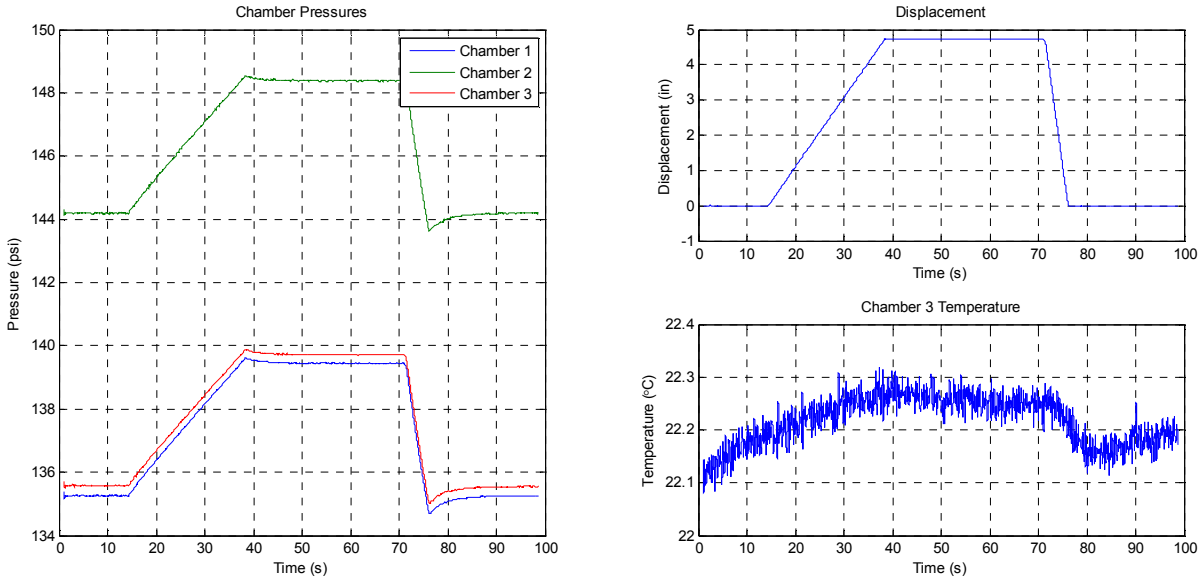

Figure 64: 120 mm Displacement